



저작자표시-비영리-변경금지 2.0 대한민국

이용자는 아래의 조건을 따르는 경우에 한하여 자유롭게

- 이 저작물을 복제, 배포, 전송, 전시, 공연 및 방송할 수 있습니다.

다음과 같은 조건을 따라야 합니다:



저작자표시. 귀하는 원저작자를 표시하여야 합니다.



비영리. 귀하는 이 저작물을 영리 목적으로 이용할 수 없습니다.



변경금지. 귀하는 이 저작물을 개작, 변형 또는 가공할 수 없습니다.

- 귀하는, 이 저작물의 재이용이나 배포의 경우, 이 저작물에 적용된 이용허락조건을 명확하게 나타내어야 합니다.
- 저작권자로부터 별도의 허가를 받으면 이러한 조건들은 적용되지 않습니다.

저작권법에 따른 이용자의 권리는 위의 내용에 의하여 영향을 받지 않습니다.

이것은 [이용허락규약\(Legal Code\)](#)을 이해하기 쉽게 요약한 것입니다.

[Disclaimer](#)

Unprecedented Insulator-To-Metal Transition  
Dynamics by Heterogeneous Catalysis in Pd-  
Sensitized Single Vanadium Oxide Nanowires

The background features a large, faint watermark of the UNIST logo. It consists of a circular emblem with the text 'UNIST NATIONAL INSTITUTE OF SCIENCE AND TECHNOLOGY' around the perimeter. Inside the circle is a shield-shaped emblem containing a stylized atomic structure with a central nucleus and orbiting electrons. Below the shield, the acronym 'UNIST' is written in a large, bold font.

Jiwon Byon

Materials Science & Engineering Program

Graduate school of UNIST

2014

Unprecedented Insulator-To-Metal Transition  
Dynamics by Heterogeneous Catalysis in Pd-  
Sensitized Single Vanadium Oxide Nanowires

Jiwon Byon

Materials Science & Engineering Program  
Graduate School of UNIST

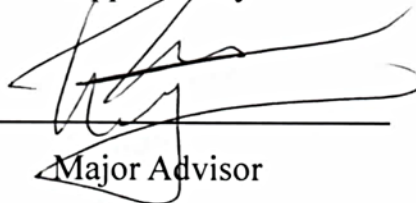
# Unprecedented Insulator-To-Metal Transition Dynamics by Heterogeneous Catalysis in Pd- Sensitized Single Vanadium Oxide Nanowires

A thesis  
submitted to the Graduate School of UNIST  
in partial fulfillment of the  
requirements for the degree of  
Master of Science

Jiwon Byon

11. 01. 2013

Approved by



---

Major Advisor

Jeong Min Baik

# Unprecedented Insulator-To-Metal Transition Dynamics by Heterogeneous Catalysis in Pd- Sensitized Single Vanadium Oxide Nanowires

Jiwon Byon

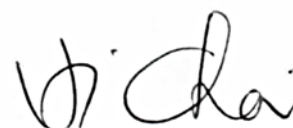
This certifies that the thesis of Jinsung Kwak is approved.

11. 01. 2013



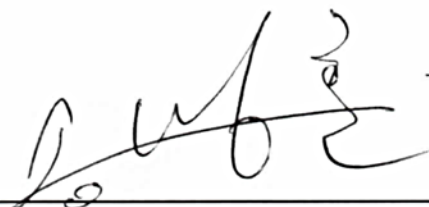
---

Thesis Supervisor: Jeong Min Baik



---

Kyoung Jin Choi: Thesis Committee Member#1



---

Myoung Hoon Song: Thesis Committee Member#2

## Abstract

In the part 1, Single crystal vanadium dioxide ( $\text{VO}_2$ ) nanowires were grown by physical vapor deposition (PVD) under atmospheric pressure and synthesized on a silicon dioxide ( $\text{SiO}_2$ ), a sapphire ( $\text{Al}_2\text{O}_3$ ) C-plan and a sapphire R-plan as a substrate. The controllable spontaneous conversion of thin films into nanowires for large area production is investigated. The synthesis is found to depend critically on the thickness of  $\text{V}_2\text{O}_5$  layer. We have controlled that the nanowires that are single crystal vanadium dioxide can be grown with thickness of  $\text{V}_2\text{O}_5$  thin film and also we can synthesize  $\text{VO}_2$  nanowires to various directions on the substrate. By using the patterned substrate, we can not only control the numerous  $\text{VO}_2$  nanowire morphologies but also fabricate the guided growth of millimeter-long  $\text{VO}_2$  nanowires.

In the part 2, we report the high effective hydrogen gas sensor based on the metal-to-insulator transition (MIT) by the electro-thermally induced Palladium-nanoparticles-decorated  $\text{VO}_2$  nanowire prepared by the efficient and size-controllable growth method originated from  $\text{V}_2\text{O}_5$  thin film driven. We have many experiments for improved hydrogen gas detector based on the MIT. First by doping the tungsten we showed that the MIT temperature was reduced to about  $40^\circ\text{C}$ . Second by irradiating a well-defined electron beam into the nanowires, we could considerably increase the conductivity up to 4 times with only a modest change in the MIT temperature ( $< 2^\circ\text{C}$ ). When exposed to trace amounts of hydrogen gas in a single nanowire configuration, the enhanced conductivity gave rise to about two times as fast transition to metallic phase even near room temperature ( $\sim 35^\circ\text{C}$ ), by reaching much faster ( $\sim 3x$ ) a critical current density at which the self-heating initiates. Last, especially Palladium- $\text{VO}_2$  nanowire near-core-shell nanostructure shows remarkably large current increase at a temperature  $10^\circ\text{C}$  lower than the MIT temperature in the bulk. This current increase occurs slowly over the duration of several seconds to several tens of seconds, depending on the Pd coverage, temperature, and hydrogen concentration. This novel finding thus mentions the capability of detecting selectively hydrogen of different three gases ( $\text{O}_2$ ,  $\text{CO}_2$ , and ethylene) and has significant implications for the effective engineering the physicochemical properties of vanadium dioxide by a heterogeneous catalytic process.

**Keywords:**  $\text{VO}_2$  nanowire, Hydrogen gas sensor, Metal-to-Insulator Transition,



# Contents

1. INTRODUCTION -----	1
1.1. CHARACTERISTIC OF VO <sub>2</sub> -----	1
1.2. MOTT TRANSITION-----	5
1.3. GROWTH METHODES OF VO <sub>2</sub> NANOWIRES-----	7
1.4. SPONTANEOUS CONVERSION OF V <sub>2</sub> O <sub>5</sub> THIN FILM INTO VO <sub>2</sub> NANOWIRES-----	8
1.5. INTERNAL-STRAIN CREATED BY HYDROGEN GAS IN Pd-VO <sub>2</sub> NEAR COR-SHELL AND APPLICATION AS GAS SENSOR-----	9
2. SPONTANEOUS CONVERSION OF V <sub>2</sub> O <sub>5</sub> THIN FILM INTO VO <sub>2</sub> NANOWIRES -----	11
2.1. EXPERIMENT-----	11
2.1.1. Experimental Equipment of VO <sub>2</sub> nanowire growth-----	11
2.1.2. Target and Substrates-----	13
2.1.3. Analysis-----	14
2.1.4. Experimental methods-----	15
2.2. RESULTS AND DISCUSSION -----	16
2.2.1. V <sub>2</sub> O <sub>5</sub> thin film fabrication-----	16
2.2.2. VO <sub>2</sub> nanowire growth with V <sub>2</sub> O <sub>5</sub> thin film thickness-----	17
2.2.3. Micro-structure analysis of grown VO <sub>2</sub> nanowire -----	18
2.2.4. Grown VO <sub>2</sub> nanowires with substrates -----	19
2.2.5. Annealing conditions of metal contact -----	20



2.2.6. Calculation of Insulator-to-Metal Transition temperature -----	21
2.2.7. Guided growth of sub-millimeter long VO <sub>2</sub> nanowires -----	22
2.2.8. VO <sub>2</sub> nanowire morphology control with patterned-substrate shapes -----	23
2.3. CONCLUSIONS -----	24
3. INTERNAL-STRAIN CREATED BY HYDROGEN GAS IN Pd-VO <sub>2</sub> NEAR COR-SHELL AND APPLICATION AS GAS SENSOR-----	25
3.1. EXPERIMENT -----	25
3.1.1. EXPERIMENT -----	25
3.1.1. Experimental equipment -----	25
3.1.2. Analysis -----	27
3.1.3. Experimental methods -----	28
3.2. RESULTS AND DISCUSSION -----	30
3.2.1. VO <sub>2</sub> nanowires doped by tungsten -----	30
3.2.2. Analysis of VO <sub>2</sub> nanowires doped by tungsten -----	31
3.2.3. Current-density change with e-beam irradiation conditions -----	32
3.2.4. Crystal structure analysis of VO <sub>2</sub> nanowires following e-beam irradiation -----	33
3.2.5. Mott transition temperatures with e-beam irradiations; I-V measurement -----	34
3.2.6. Mott transition temperatures with e-beam irradiations; Raman Spectra -----	35
3.2.7. Sensing performance with e-beam irradiation conditions -----	36
3.2.8. Detecting hydrogen gas at the room temperature -----	38

3.2.9. The selectivity of different four gases -----	39
3.2.10. The temperature coefficient of resistance-----	40
3.2.11. VO <sub>2</sub> nanowire temperature calculation by COMSOL multiphysics package -----	41
3.2.12. Induced defects from high e-beam energy -----	43
3.2.13. SEM & TEM images of palladium deposited & non-deposited VO <sub>2</sub> nanowires -----	44
3.2.14. Response rate with palladium thickness -----	45
3.2.15. Response rate with hydrogen concentration -----	47
3.2.16. Response rate with palladium distance -----	48
3.2.17. Phase transition in VO <sub>2</sub> due to localized heating via Pd-H reaction -----	50
3.2.18. Two recovery methods following hydrogen flow -----	54
3.2.19. Sensing performance at the low voltage and room temperature -----	56
3.3. CONCLUSIONS -----	57
REFERENCES -----	58
ACKNOWLEDGEMENT	

## List of figures

Figure 1.1 Phase transition of vanadium dioxide (adapted from ref. 5) -----	1
Figure 1.2 Phase diagram in stress (adapted from ref. 14) -----	2
Figure 1.3 Raman spectra with Vanadium dioxide nanowire phase(adapted from ref. 15) -----	3
Figure 1.4 Temperature-dependent optical transmission of VO <sub>2</sub> (adapted from ref. 16) -----	4
Figure 1.5 a) the curve is the effective mass of quasi-particle, b) The system becomes inhomogeneous due to doped holes (adapted from ref. 24) -----	6
Figure 1.6 Schematic drawing of spontaneous conversion of V <sub>2</sub> O <sub>5</sub> thin film into VO <sub>2</sub> nanowires -----	7
Figure 2.1 Radio Frequency Sputter (RF-sputter) -----	11
Figure 2.2 Atmospheric-pressure, Physical Vapor Deposition (APPVD) -----	12
Figure 2.3 a)Thermally grown SiO <sub>2</sub> layer with 2000 Å thickness on a polished Si(100) single crystal, b) Patterned substrate on a polished Si(100) single crystal, c) Vanadium target (99.99 %), d) Sapphire (Al <sub>2</sub> O <sub>3</sub> ) C-Plane, e) Sapphire (Al <sub>2</sub> O <sub>3</sub> ) R-Plane, f) Schematic structure of sapphire (Al <sub>2</sub> O <sub>3</sub> )-----	13
Figure 2.4 Schematic drawing of Patterned substrate process for fabricating the numerous VO <sub>2</sub> nanowire morphologies and the guided growth of millimeter-long VO <sub>2</sub> nanowires -----	15
Figure 2.5The control of O <sub>2</sub> partial pressure led to the formation of V <sub>2</sub> O <sub>5</sub> thin film on the sapphire substrate -----	16
Figure 2.6SEM images (scale bar = 10 μm) of as-grown VO <sub>2</sub> nanowires grown on SiO <sub>2</sub> substrateswith varying thickness of V <sub>2</sub> O <sub>5</sub> film from 2 to 20 nm. Inset in (b) shows the representative image of VO <sub>2</sub> nanowires obtained at 5 nmthick-sample-----	17
Figure 2.7 (a) XRD diffraction of VO <sub>2</sub> nanowires on a SiO <sub>2</sub> /Si substrate. The VO <sub>2</sub> peaks are observed at the (011) and (022) reflections. (b) Raman spectra of a VO <sub>2</sub> single nanowire on a sapphire substrate. The optical image shows that the laser spot was focused on a VO <sub>2</sub> -nanowire center. Peaks of Raman spectra are shown by sharp peaks at 197 and 225 cm <sup>-1</sup> and broad peak at 630cm <sup>-1</sup> -----	18
Figure 2.8 (a) Low magnification SEM image of VO <sub>2</sub> nanowires and cross-section image on a polished SiO <sub>2</sub> /Si substrate, (b) The grown VO <sub>2</sub> nanowires on a non-polished SiO <sub>2</sub> /Si substrate, (c) VO <sub>2</sub> nanowires on r-plane sapphire and an angle of 60° from the floor, (d) High magnification TEM images of single VO <sub>2</sub> nanowire -----	19
Figure 2.9 Current-voltage curves with the annealing temperatures and VO <sub>2</sub> nanowire condition after an annealing over 500 °C-----	20
Figure 2.10(a) I-V curves measured at ambient temperature in the range of 45 - 53 °C by varying the applied bias both from low to high voltage values and in the reverse direction of as-grown	

VO <sub>2</sub> nanowires, (b) A plot of the difference in the square of the voltages at which the Mott transition occurs in the upward and downward directions vs ambient temperature ( $\Delta V_M^2$ vs T), (c) Heating and cooling temperatures, observed peak ratio of Raman spectra. Raising temperatures, peak of Raman spectra disappeared-----	21
Figure 2.11 Optical and SEM image of sub-millimeter long VO <sub>2</sub> nanowire -----	22
Figure 2.12 The cross-section shapes of VO <sub>2</sub> nanowires, (a) diamond-shaped, (b) rectangular-shaped, (c) hexagonal-shaped, (d) round-shaped. The cross-section shapes of VO <sub>2</sub> nanowires are decided by the shapes of bowls, because the solid V <sub>2</sub> O <sub>5</sub> thin films melt to liquid V <sub>2</sub> O <sub>5</sub> nanodroplets -----	23
Figure 3.1 E-beam evaporator, Pd nanoparticle and electrode, Au/Ti (200/20nm) deposition -----	25
Figure 3.2 Schematic drawing of high voltage electron beam accelerator -----	26
Figure 3.3 Customized current-voltage measurement systems -----	27
Figure 3.4 SEM images of VO <sub>2</sub> nanowires doped by tungsten -----	30
Figure 3.5 (a) substrate and VO <sub>2</sub> nanowire and W-doped VO <sub>2</sub> nanowire of Raman spectra, (b) Heating temperatures, observed peak ratio of Raman spectra. Raising temperatures, peak of Raman spectra disappeared, (c) 2.5% W-doped EDX result -----	31
Figure 3.6 Change in current density of VO <sub>2</sub> nanowires as a function of e-beam irradiation power and dose -----	32
Figure 3.7 Bright-field images (scale bar = 100 nm), and HR-TEM images (scale bar = 5 nm), and the corresponding Fast Fourier Transformed (FFT) diffraction patterns of VO <sub>2</sub> nanowires as a function of e-beam irradiation power and dose; (a) as-grown (b) 0.5 MeV, 10 <sup>16</sup> /cm <sup>2</sup> (c) 0.7 MeV, 10 <sup>14</sup> /cm <sup>2</sup> -----	33
Figure 3.8 (a) I-V curves measured at ambient temperature in the range of 45 - 53 °C by varying the applied bias both from low to high voltage values and in the reverse direction of as-grown VO <sub>2</sub> nanowires, (b) A plot of the difference in the square of the voltages at which the Mott transition occurs in the upward and downward directions vs ambient temperature ( $\Delta V_M^2$ vs T), (c) The Mott transition temperatures as a function of e-beam irradiation energy and dose (inset) A plot of the difference in the square of the Voltages after e-beam irradiation of 0.5 MeV at dose of 10 <sup>16</sup> /cm <sup>2</sup> and after e-beam irradiation of 0.7 MeV at dose of 10 <sup>14</sup> /cm <sup>2</sup> -----	34
Figure 3.9 Mott transition temperatures with irradiation conditions. Raman peak (197 cm <sup>-1</sup> ) was observed by heating and cooling a VO <sub>2</sub> nanowire-----	35
Figure 3.10 (a) The change in current for a Pd-decorated as-grown VO <sub>2</sub> nanowire biased at 10 V as a function of time of exposure to hydrogen gas, (b) The change in current as a function of e-beam irradiation energy (0.5 MeV: red and blue curves, 0.7 MeV: green curve) and dose, (c) The response time as a function of e-beam irradiation energy. The open square is a result of response time measured when the Pd thickness is increased to 2.5 nm-----	37
Figure 3.11 The change in current for a Pd-decorated as-grown VO <sub>2</sub> nanowire biased at 10 V as a	

function of time of exposure to hydrogen gas with e-beam irradiation energy and dose, measured at 35 °C and 40 °C-----	38
Figure 3.12 The selectivity of sensors in detecting hydrogen gas of different four gases (H <sub>2</sub> , O <sub>2</sub> , CO, and ethylene). Inset shows the CO response measured at 60 °C -----	39
Figure 3.13 Plots of LnI vs. 100/T of VO <sub>2</sub> under Ar, Pd-VO <sub>2</sub> under ar and H <sub>2</sub> -----	40
Figure 3.14 (a) 3D model in COMSOL of a VO <sub>2</sub> nanowire (lateral dimension: 70x 100 nm) on a SiO <sub>2</sub> /Si substrate (Inset shows the SEM image of the VO <sub>2</sub> nanowire), (b) Plots of ΔT versus distance along the axis of the nanowire shown in (a) measured at 5V as a function of e-beam irradiation power and dose. (c) temperature difference of nanowires before H <sub>2</sub> exposure and near MIT as a function of e-beam irradiation power and dose -----	42
Figure 3.15 I-V curve and SEM image of Pd-VO <sub>2</sub> after e-beam irradiation at 0.7 MeV. This information is available free of charge via the Internet at <a href="http://pubs.acs.org">http://pubs.acs.org</a> -----	43
Figure 3.16 (a) Low magnification SEM image of VO <sub>2</sub> nanowires, (b) Low magnification and (c) high magnification TEM images of single VO <sub>2</sub> nanowire, (d) SEM image of single nanowire spanning gold contacts separated by about 15 μm. Low magnification, (e) and high magnification (f) SEM images of Pd-decorated single VO <sub>2</sub> nanowire. The scale bar is 10 μm, 200 nm, 2 nm, 100 nm, 5 μm, and 500 nm respectively-----	44
Figure 3.17(a) The change in current for a Pd-decorated VO <sub>2</sub> nanowire biased at 5 V as a function of time of exposure to hydrogen gas with Pd film thickness (1 – 3 nm). The scale bar in the inset is 100 nm. As the Pd thickness is increased from 1 to 3 nm, the hydrogen response becomes faster.(b) The details of the current change of Pd-VO <sub>2</sub> nanowire, exposed to hydrogen flowing at 5 sccm added for various lengths of time to a 1000 sccm background air stream with the thickness of Pd films-----	46
Figure3.18(a) I <sub>D</sub> curves for a Pd-decorated VO <sub>2</sub> nanowireat 50 °C exposed to varying hydrogen partial pressures in dry air corresponding to concentrations ranging from 250 ppm to 5000 ppm. (b) The rate of increase in a current with hydrogen concentration-----	47
Figure 3.19 Response time with the H <sub>2</sub> concentration of 500 and 5000 ppm with Pd coverage-----	49
Figure 3.20(a) The snapshots of temperature and induced compressive stress distributions of VO <sub>2</sub> nanowire by Pd-H exothermal reaction. (b) The profiles of temperature, induced compressive stress, and conductivity of VO <sub>2</sub> nanowires with different length-----	52
Figure 3.21Comparison of temperature profiles of VO <sub>2</sub> nanowires decorated by a Pd thin film and Pd nanoparticles in (a) and that decorated by 10nm size Pd nanoparticles and 200nm size Pd nanoparticles in (b) The profiles of temperature and conductivity for different amount of heat sources per a single Pd atom in (c) and those for different sizes and inter-distances of Pd nanoparticles in (d)-----	53
Figure 3.22 Two types of recovery process, heat the sample at 100 ~ 200 °C (a) and stretching the	

sample (b)----- 54

Figure 3.23The change in current for a Pd-decorated VO<sub>2</sub> nanowire after hydrogen off with annealing temperature----- 55

Figure 3.24The change in current for a Pd-decorated VO<sub>2</sub> nanowire biased at 10 V with exposure to hydrogen gas at room temperature (a) a Pd-decorated VO<sub>2</sub> nanowire biased at 0.1 V at 50 °C (b)----- 56

## List of table

Table 1 Dimension, electrical and thermal conductivity of VO<sub>2</sub> nanowire and SiO<sub>2</sub> substrate ----- 41

# 1. Introduction

## 1.1. CHARACTERISTIC OF VO<sub>2</sub>

Vanadium is expressed by chemical element with the symbol V and atomic number 23. It is silvery gray and malleable transition metal. Vanadium element is found only in chemically combined with oxide in nature. Vanadium combined with oxygen shows such as V<sub>2</sub>O<sub>5</sub>, V<sub>2</sub>O<sub>3</sub>, VO<sub>2</sub>, and so on. On vanadium combined with oxygen, vanadium dioxide (VO<sub>2</sub>), a strongly correlated electron material, undergoes a Mott metal-insulator transition (MIT) with extremely change in electronic and optical properties at a temperature of 68 °C in the bulk.<sup>[1-4]</sup>In general, the Mott transition in vanadium dioxide (VO<sub>2</sub>) occurs alongside a structural phase transition from monoclinic (M1, the insulator or semiconductor phase) at temperatures below the Mott transition temperature to tetragonal (R, the metallic phase) above that temperature, which is accompanied by several orders of magnitude jump in conductivity (Figure 1.1).

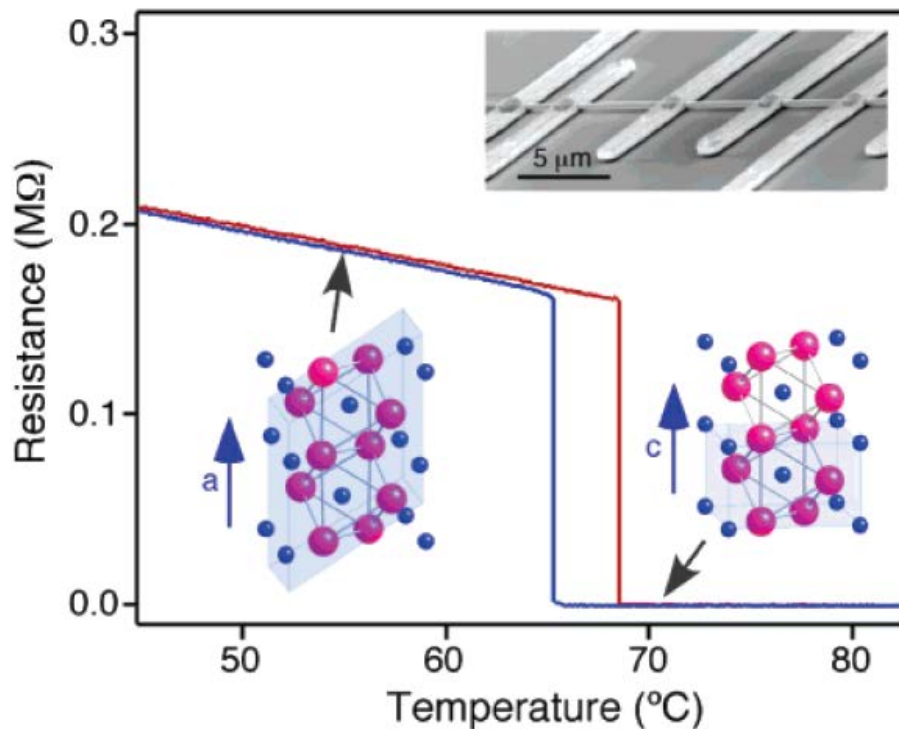


Figure 1.1 Phase transition of vanadium dioxide (adapted from ref. 5)



Vanadium dioxide ( $\text{VO}_2$ ) is highly concerned with electron material which exhibits a metal-to-insulator transition (MIT) coupled with rutile (R) of tetragonal (the metallic phase) – monoclinic (M1, the insulator or semiconductor phase) structural transition.<sup>[6,7]</sup> It is known that the metal-to-insulator transition (MIT) temperature and domain structure are completely affected by uniaxial strains. The metal-to-insulator transition (MIT) can be further complicated at large strain or high Cr doping that induces another monoclinic structure of  $\text{VO}_2$ , the M2 phase (Figure 1.2).<sup>[8-12]</sup> In recent studies, vanadium dioxide ( $\text{VO}_2$ ) has been known that the compressive strain (2.2%) can totally complete the transition of a  $\text{VO}_2$  nanowire to the metallic phase at room temperature.<sup>[13]</sup> However, the electronic nature of the transitions between the M1, M2, and R structural phase has not been explained across the broad phase space.<sup>[14]</sup>

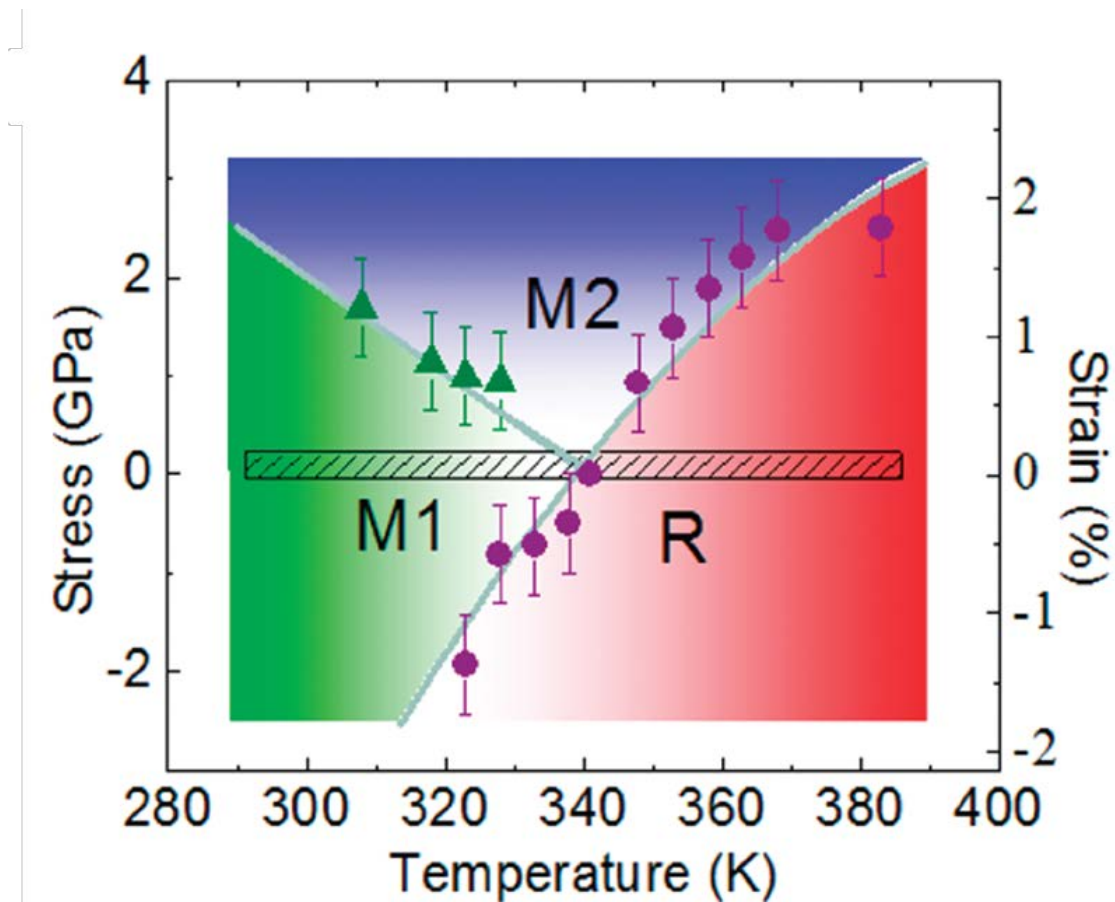


Figure 1.2 Phase diagram in stress (adapted from ref. 14).

Insulator phase M1 and M2 and metallic phase R of vanadium dioxide nanowire distinguished by

Raman spectra.<sup>[15]</sup> Raman spectra was measured by heating the vanadium dioxide nanowire. Figure 1.3<sup>[15]</sup> shows insulating phase M1 and M2 and metallic phase R of the Raman spectra peak. Raman spectra was changed from 608  $\text{cm}^{-1}$  (M1 phase) to 645  $\text{cm}^{-1}$  (M2 phase) of broad peak, increasing the temperature and then all of the peak of Raman spectra disappeared, changing the metallic phase of vanadium dioxide.

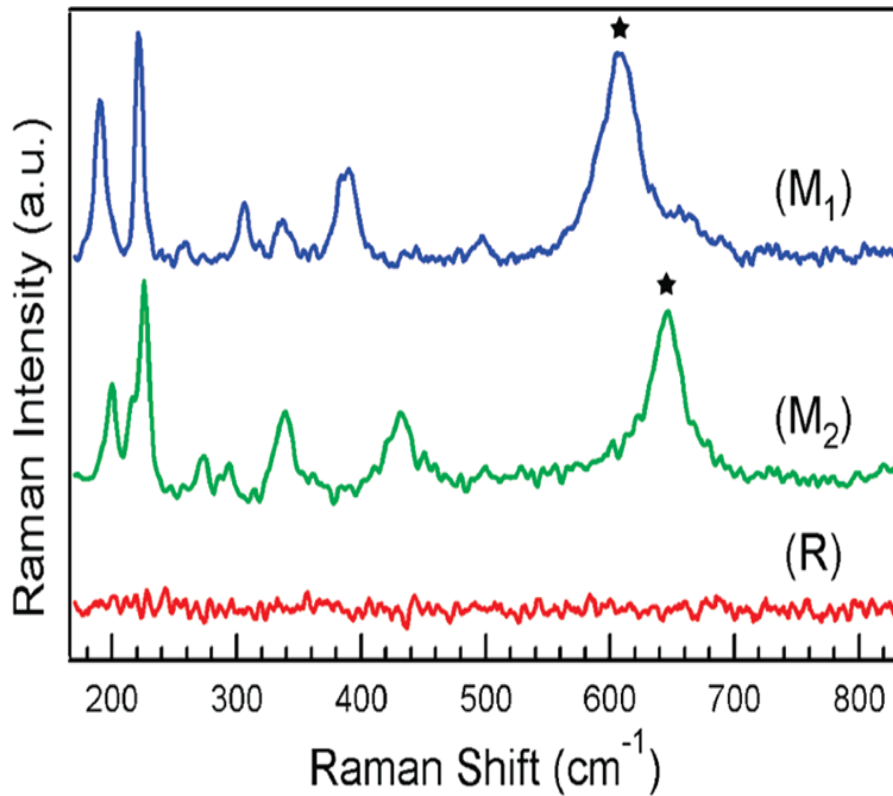


Figure 1.3 Raman spectra with Vanadium dioxide nanowire phase (adapted from ref. 16).

Also, optical properties of vanadium dioxide ( $\text{VO}_2$ ) are changed by transferring the phase from insulator to metal. The optical transmittance depends on the temperature that modifies vanadium dioxide ( $\text{VO}_2$ ) phase. Figure 1.3 shows the temperature-dependent optical transmission (at the wavelength of 2500 nm) and thermal hysteresis loop of vanadium dioxide ( $\text{VO}_2$ ).<sup>[16]</sup> When vanadium dioxide ( $\text{VO}_2$ ) is heated and cooled, vanadium dioxide ( $\text{VO}_2$ ) undergoes a different phase transition with a transmittance gap of  $\Delta Tr = 53\%$  at  $\lambda = 2500 \text{ nm}$  and shows the feature hysteretic behavior with  $\Delta T = 9.8 \text{ }^\circ\text{C}$  (figure 1.3). The hysteresis is relevant to the multidomain vanadium dioxide ( $\text{VO}_2$ ) structure, nanosized vanadium dioxide crystals, and other parameters.<sup>[17-19]</sup>

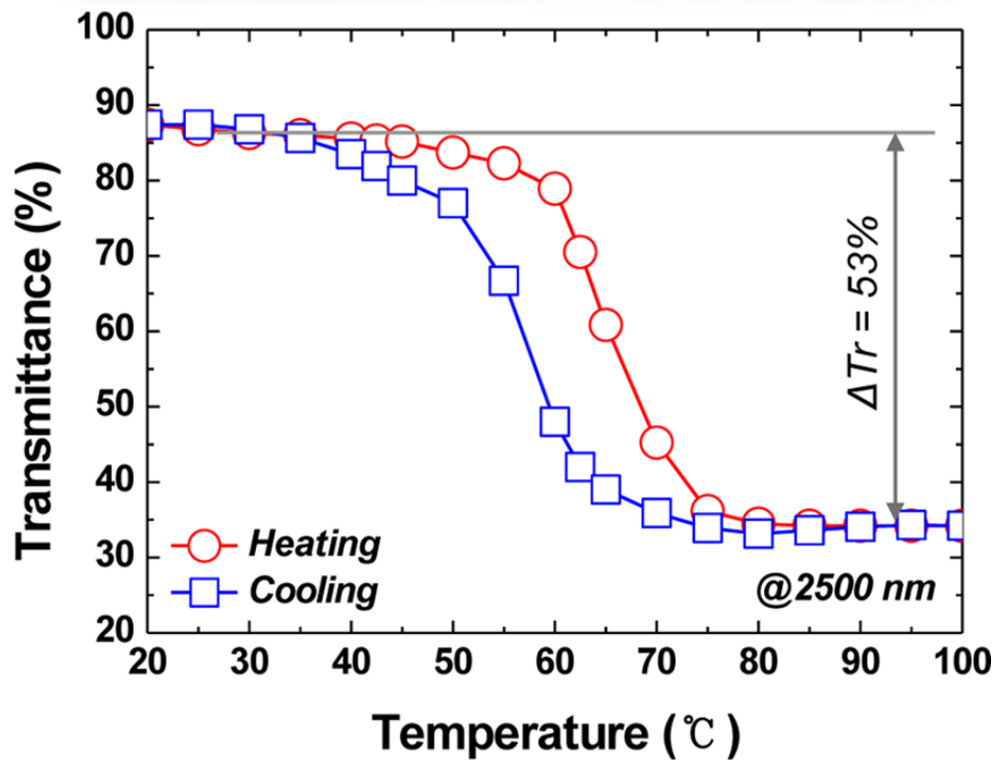


Figure 1.4 Temperature-dependent optical transmission of  $\text{VO}_2$  (adapted from ref. 16).

## 1.2.MOTT TRANSITION

Mott transition was first proposed by Nevill Francis Mott who was an English physicist and won the Nobel Prize for Physics in 1977. He assumed playing around electron correlations including nickel oxides that could change from metals to insulators under various physical conditions. Simply, Mott transition is from the insulator to the metal of a material. This theory is due to the electron density and electric field screening of the coulomb potential changes.<sup>[20,21]</sup> If a material gets small electron density, it will be weak screening. Therefore, the electrons are bound and the material is an insulator. If a material becomes large electron density, the electrons will be no bound states and the material will be a metal due to the strong screening. To undergo a Mott transition, a material needs to have a sufficient electron density.

Hyun Tak Kim from ETRI argued the hole-driven MIT theory<sup>[22]</sup> which is the extension of the Brinkman-Rice picture.<sup>[23]</sup> To demonstrate the hole-driven MIT, he observed inhomogeneous VO<sub>2</sub> film.

On the basis of the fractional charge, the fractional Coulomb energy is defined as  $U \equiv \langle e'e'/r \rangle = \rho^2 U_{\text{true}}$ , where  $U$  is the effective Coulomb energy and  $U_{\text{true}}$  is the true Coulomb energy. For a given  $U_c$ ,  $U_{\text{true}} = \kappa U_c$  is given, where  $\kappa$  is the correlation strength used in the BR picture.<sup>[23]</sup>

For an averaged system with one effective charge per atom, the effective mass of a quasi-particle  $m^*$ , calculated by the Gutzwiller variational theory<sup>[22]</sup>, is given by

$$\frac{m^*}{m} \equiv \frac{1}{1 - (U/U_c)^2} = \frac{1}{1 - \kappa^2 \rho^4}$$

Where  $m$  is the bare electron mass,  $U/U_c$  is  $\kappa \rho^2 \neq 1$ ,  $\kappa$  is the strength of Coulomb energy.

In the vanadium dioxide, a metal to insulator transition near  $U/U_c = 1$  occurs suddenly with inhomogeneity by semi-conduction as a doping process of internal holes of  $n_c \approx 0.018\%$ . Hole doping of a low concentration to a Mott insulator causes a breakdown of on-site Coulomb energy from  $U_c$  to a large constant  $U (< U_c)$ , as indicated in figure 1.4.<sup>[22, 24]</sup>

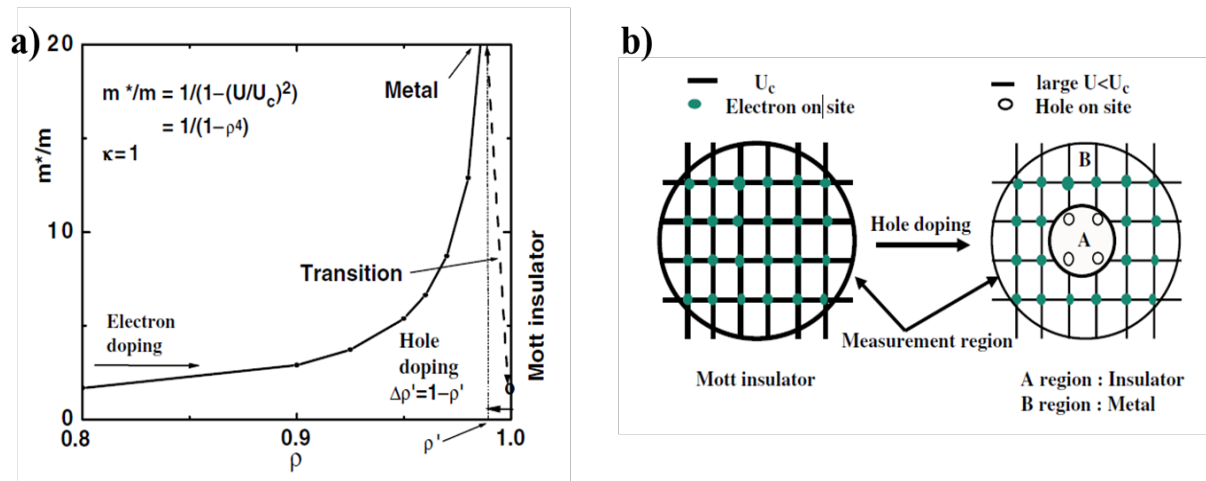


Figure 1.5 a) the curve is the effective mass of quasi-particle, b) The system becomes inhomogeneous due to doped holes (adapted from ref. 24).

### 1.3.GROWTH METHODES OF VO<sub>2</sub> NANOWIRES

There are many methods for growing VO<sub>2</sub> nanowires such as hydro-thermal method, CVD process, and PVD process, etc. Among some methods, we selected Atmospheric Pressure Physical Vapor Deposition (APPVD) process.

First, we fabricated V<sub>2</sub>O<sub>5</sub> thin film simply using a radio-frequency (RF) reactive sputtering chamber with vanadium target (99.99%), flowing argon (16sccm) /oxygen (4sccm) mixtures under the operating pressure of 4mTorr and substrate temperature of 450 °C, the V<sub>2</sub>O<sub>5</sub> thin films were deposited onto the substrates.

Then, the fabricated thin films were moved into the middle of a 1 inch horizontal quartz tube furnace to grow VO<sub>2</sub> nanowires under atmospheric pressure. The synthesis was implemented during 2 hours at 650 °C with flowing high purity He gas (99.999%) at 300 sccm. When raising temperature at 500 °C, the He gas (99,999%) at 300 sccm was flowing 1 inch horizontal quartz tube (figure 1.6).

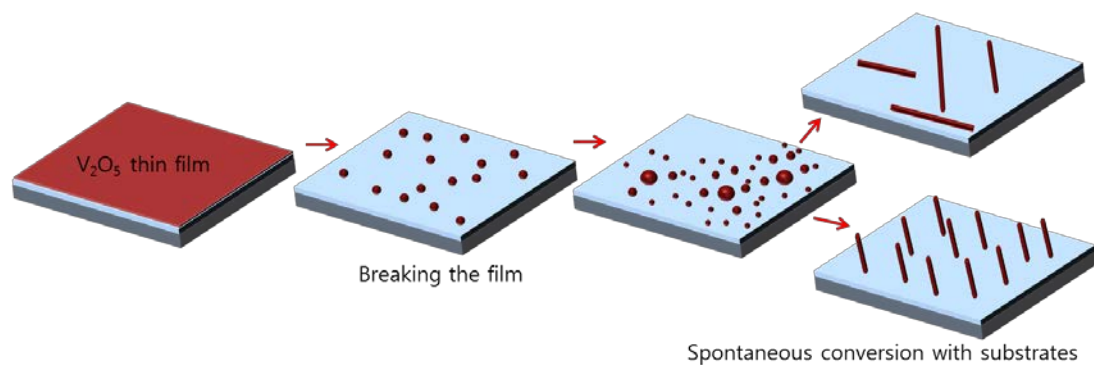


Figure 1.6 Schematic drawing of spontaneous conversion of V<sub>2</sub>O<sub>5</sub> thin film into VO<sub>2</sub> nanowires.

#### 1.4. SPONTANEOUS CONVERSION OF $V_2O_5$ THIN FILM INTO $VO_2$ NANOWIRES

The quasi 1-Dimensional nanostructures like semiconducting nanowires have been extensively explored toward their potential utility in optoelectronics, sensors, nanoelectronics, and electrochemical energy conversion and storage devices<sup>[25-27]</sup> The various methods of synthesizing nanowires have been developed to effectively fabricate metallic and semiconductor nanowires with unique physicochemical properties, including liquid phase self-assembly, template growth on nanometer sized pores, and chemical vapor deposition with or without metal catalysts. Recently, it was newly reported that  $Bi_2Te_3$  and Bi nanowires are grown via direct “OFF-ON” synthesis mode in a simple manner using the thermally induced stress of a thin precursor film.<sup>[28]</sup> In this process, they suggested that the synthesis of the nanowire could be induced by atomic diffusion of components of the thin film along grain boundaries in the presence of compressive stress. Although various crystal growth methods are well established in preparing nanowires of high crystallinity as well as high aspect ratio, it is still challenging to control making high quality nanowires with the uniform size and length for real applications.

In this part we report an exceptionally simple and effective strategy to fabricate uniform nanowires by spontaneous conversion of thin film. We suggest that the  $VO_2$  nanowires with extremely narrow size and length distributions can be successfully grown on a numerous substrates through the complete dewetting process from the thin film of the  $V_2O_5$  Phase. Also we can control the  $VO_2$  nanowire morphologies with various patterned substrates.

## 1.5. INTERNAL-STRAIN CREATED BY HYDROGEN GAS IN Pd-VO<sub>2</sub> NEAR COR-SHELL AND APPLICATION AS GAS SENSOR

Quasi-one-dimensional (1-D) nanostructures have been extensively explored due to their potential utilities in optoelectronics, sensors, electronics, and energy conversion and storage devices.<sup>[29-31]</sup> Vanadium dioxide (VO<sub>2</sub>), a strongly correlated electron material, undergoes a Mott metal-insulator transition (MIT) at a temperature of 68 °C in the bulk.<sup>[1-4]</sup> In general, the Mott transition in VO<sub>2</sub> occurs alongside a structural phase transition from monoclinic (the insulator or semiconductor phase) at temperatures below the Mott transition temperature to tetragonal (the metallic phase) above that temperature, which is accompanied by several orders of magnitude jump in conductivity. Other than the temperature, external strain, light, and doping can significantly affect the phase transition by changing the transition temperature or the phase stability.<sup>[32-37]</sup> Many efforts have been thus devoted to this material due to their potential applications in Mott transition field-effect transistors, switching and metamaterial device, sensors, and smart windows.<sup>[38-40]</sup>

To date, many chemical sensors based on novel metal nanoparticles and semiconductor oxides such as tin oxide, tungsten oxide, titanium dioxide, etc., have been reported.<sup>[41-44]</sup> However, a major disadvantage is that these sensors operate only at temperatures greater than 100°C (may show low sensitivity at lower temperatures), thus resulting in higher power consumption and a reduction in their stability. On the contrary, a VO<sub>2</sub> based MIT sensor is able to operate at temperatures lower than the MIT temperature of (~ 68 °C) and can show ultra-high sensitivity of ~ 1000 fold enhancement.<sup>[31, 38]</sup> In particular, if VO<sub>2</sub> nanostructures can be properly combined with catalytic nanoparticles interacting strongly with specific gases, it can be a very promising direction to realize a superior gas sensor with ultra-sensitive and selective response for various gases.

There has long been interested in the influence of chemical doping on the insulator to metal transition of VO<sub>2</sub>. It is well-known that the transition temperature can be lowered by incorporation of foreign atoms such as W, Ti and is strongly dependent on the stoichiometry of VO<sub>2</sub>.<sup>[45-47]</sup> Very recent hydrogenation experiments on the VO<sub>2</sub> nanowires have also shown that hydrogen in VO<sub>2</sub> promotes the electronic and structural phase transition at lower temperature than 68 °C because of the decrease in the energy bandgap by lowering the  $\pi^*$  level in energy band diagram.<sup>[48]</sup> Actually, hydrogen in VO<sub>2</sub> can act as an electron donor increasing the carrier density in the conduction band, causing a shift in insulator to metal transition temperature.<sup>[36-38, 49]</sup> Hydrogen gas at high temperature (~ 400 °C) also reduces the oxides, resulting in compositional variation and leading to the structural change from monoclinic to hexagonal close packed (hcp) structure.<sup>[50]</sup> However, most of works was



conducted at higher temperature than the transition temperature.

Here, we introduced that raising the conductivity can considerably promote the transition to the metallic phase by responding to the critical electron concentration (for Joule self-heating) faster ( $>2x$ ). For increasing the conductivity, we implemented an electron beam intentionally to alter the surface structure of  $\text{VO}_2$  with very little change in MIT temperature ( $< 2\text{ }^\circ\text{C}$ ). Although e-beam irradiation technique can also induce local composition deviations in material stoichiometry, these side effects could be minimized by finding a way for an effective use of e-beam irradiation in material properties. The sensor is then tested for the capability of selectively detecting hydrogen from the following these gases ( $\text{O}_2$ ,  $\text{CO}$ , and ethylene).

Also, we report an unusual insulator to metal transition of the palladium-decorated  $\text{VO}_2$  nanowires caused by the heterogeneous  $\text{H}_2$ -Pd catalytic reactions. With exposure to hydrogen, the  $\text{VO}_2$  exhibits an insulator to metal transition at  $50\text{ }^\circ\text{C}$ , lower than the transition temperature in the bulk. The transition occurs slowly over duration of several seconds to several tens of seconds, depending on the Pd coverage, temperature, and hydrogen concentration, which is not usually observed in the first-order metal-insulator transition of single crystalline  $\text{VO}_2$ . Here, we discuss electronic transport with various experimental conditions such as hydrogen concentration, temperature, Pd coverage, and applied voltage, and perform finite element analyses using COMSOL Multiphysics software. These experiments allow us to examine the deceleration in the transition in terms of the catalytic reactions in detail. After hydrogen flow is shut off, the conductance is not immediately returned to the original value and it takes approximately 30 min even after  $100\text{ }^\circ\text{C}$ , meaning that the atomic hydrogens, produced by dissociative chemisorption on Pd, are incorporated into  $\text{VO}_2$ . However, the Pd-decorated  $\text{VO}_2$  nanowire after the recovery process also shows similar current response to hydrogen gas, meaning that it is reversible.

## 2. SPONTANEOUS CONVERSION OF $V_2O_5$ THIN FILM INTO $VO_2$ NANOWIRES

### 2.1. EXPERIMENT

#### 2.1.1 Experimental Equipment of $VO_2$ nanowire growth

For fabricating the  $V_2O_5$  thin film, we used a RF reactive Sputter (Figure 1.1). The system is composed of a load-lock chamber and a main chamber so that vacuum of main chamber is maintained and protected from possible contamination by preventing it from being directly exposed in air. The load-lock chamber is contacted by a rotary pump to the base pressure of  $\sim 1 \times 10^{-3}$  Torr and the main chamber is equipped with a turbo-molecular pump to the base pressure of  $\sim 1 \times 10^{-6}$  Torr.



Figure 2.1 Radio Frequency Sputter (RF-sputter).

To grow the nanowire of  $\text{VO}_2$ , we used an atmospheric-pressure and physical vapor deposition (APPVD). The APPVD is equipped with heating system to  $1200\text{ }^\circ\text{C}$  and Photograph is in Figure 1.2. The system is included in a 1 inch horizontal quartz tube furnace, a temperature controller, and mass flow controller (MFC). We can be able to flow three gases ( $\text{He}$ ,  $\text{H}_2$ ,  $\text{N}_2$ ) in a 1 inch horizontal quartz tube furnace.

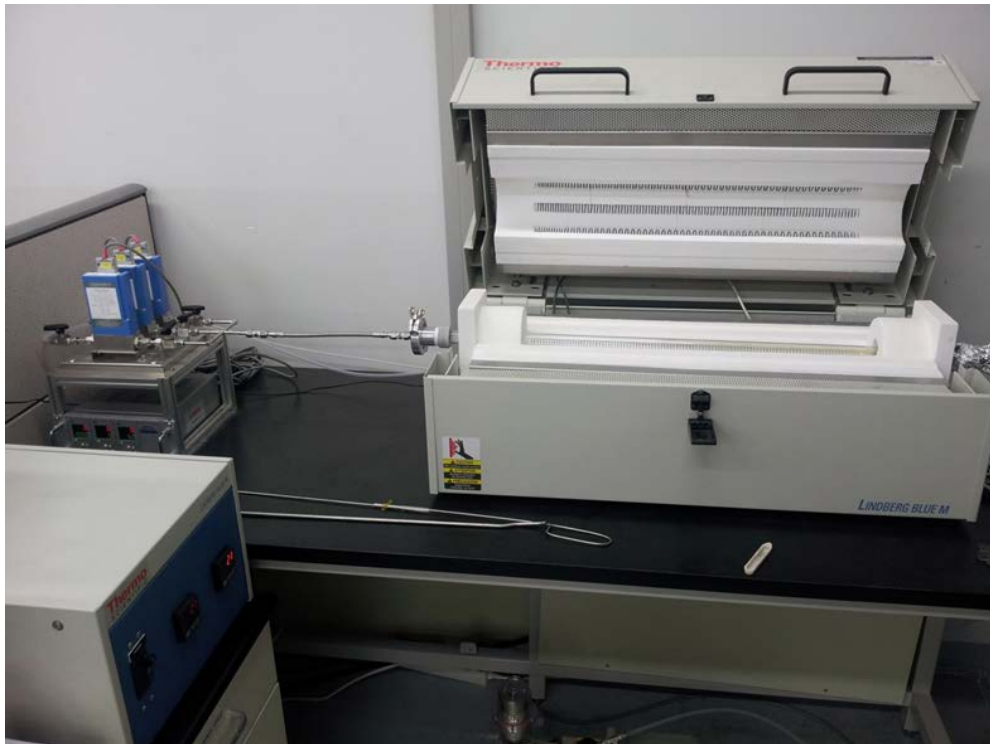


Figure 2.2 Atmospheric-pressure, Physical Vapor Deposition (APPVD).

### 2.1.2. Target and Substrates

The  $V_2O_5$  thin films were deposited onto a thermally grown  $SiO_2$  layer with  $2000\text{ \AA}$  thickness and resistivity of  $1\text{-}30\ \Omega\cdot\text{cm}$  on a polished  $Si(100)$  single crystal, non-polished  $Si(100)$  single crystal,  $Al_2O_3$  c-plan,  $Al_2O_3$  r-plan, and patterned substrate on  $Si(100)$ . Patterned substrates were fabricated using  $O_2$  plasma. First, PDMS/N-Hexane was coated by spin casting on substrates, and PDMS or Glass stamped imprinting ( $550\text{nm}$ ). Then, stamped substrates were exposed by  $O_2$  plasma. To fabricate  $V_2O_5$  thin film we used vanadium target ( $99.99\%$ ) for RF-sputter.

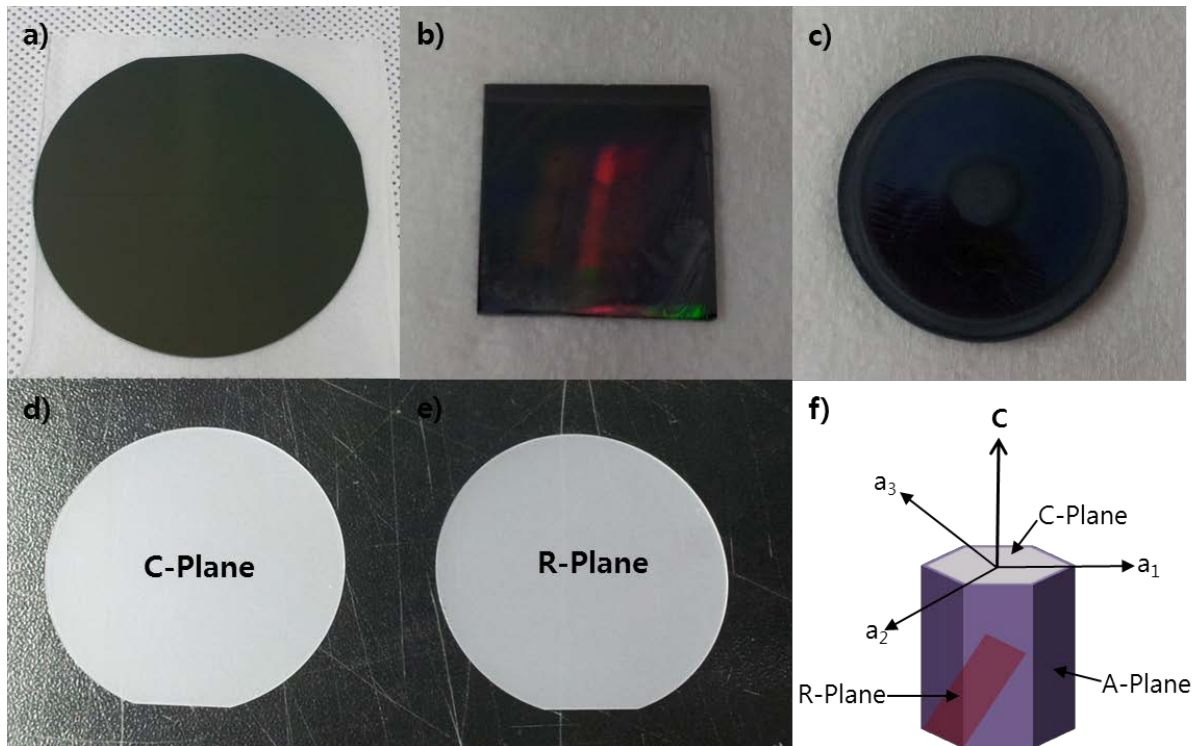


Figure 2.3 a) Thermally grown  $SiO_2$  layer with  $2000\text{ \AA}$  thickness on a polished  $Si(100)$  single crystal, b) Patterned substrate on a polished  $Si(100)$  single crystal, c) Vanadium target ( $99.99\%$ ), d) Sapphire ( $Al_2O_3$ ) C-Plane, e) Sapphire ( $Al_2O_3$ ) R-Plane, f) Schematic structure of sapphire ( $Al_2O_3$ ).

### 2.1.3. Analysis

After the growth of VO<sub>2</sub> nanowires, VO<sub>2</sub> nanowires were confirmed by Raman spectroscopy that is method for analyzing VO<sub>2</sub> in comparison with other composites. The Raman spectra were implemented with WiTec alpha 300R M-Raman system with 532 nm (2.23 eV) excitation. The laser spot size was ~ 500 nm in diameter with a 50× optical lens. When measuring the VO<sub>2</sub> nanowire to prevent deformation or damage of a VO<sub>2</sub> nanowire from laser-induced heating, we had the laser power of 0.15 mW maintained.

The crystallinity of VO<sub>2</sub> nanowires was confirmed by using a high resolution X-ray diffractometer (Bruker, D8 Advance, Germany), which is equipped with a dual channel asymmetrically cut monochromator on motorized slide. It was operating at 40 kV and 40 mA. Nickel-filtered Cu K<sub>α</sub> radiation was used in the incident beam ( $\lambda = 1.5418 \text{ \AA}$ ), which is focused on the line shape. Diffractograms were recorded at room temperature in the range  $2\theta = 20 - 60^\circ$  with a step of  $2^\circ/\text{min}$ .

To observe morphology of the VO<sub>2</sub> nanowire, Field Emission Scanning Electron Microscopy (FE-SEM) was carried out by using a Nano 230 of FEI that includes a Schottky type thermal field emission gun and provides 1.0 nm microscope resolution at 15 kV, magnification range of 30 – 800,000 x. The probe current is from 0.6 pA to 100 nA.

The high-resolution transmission electron microscopy (HRTEM) images were performed by using a Cs-corrected JEOL JEM-2100F TEM operated at 200 keV. A Gatan Multiscan CCD camera was used for the image acquisition with a pixel size of  $1024 \times 1024$ .

#### 2.1.4. Experimental methods

Single crystalline vanadium oxide nanowires were fabricated using atmospheric pressure, physical vapor deposition. Simply, using a radio-frequency (RF) reactive sputtering chamber with vanadium target (99.99%), flowing argon (16sccm) /oxygen (4sccm) mixtures under the operating pressure of 4mTorr and substrate temperature of 450 °C, the  $V_2O_5$  thin films were deposited onto a thermally grown  $SiO_2$  layer with 2000 Å thickness on a polished Si(100) single crystal, non-polished Si(100) single crystal,  $Al_2O_3$  c-plan, and  $Al_2O_3$  r-plan substrate. The thickness of the thin films was controlled by adjusting the deposition time (2, 5, 10, and 30min). Then, the fabricated thin films were moved into the middle of a 1 inch horizontal quartz tube furnace to grow  $VO_2$  nanowires under atmospheric pressure. The synthesis was implemented during 2 hours at 650 °C with flowing high purity He gas (99.999%) at 300 sccm. When raising temperature at 500 °C, the He gas (99,999%) at 300 sccm was flowing 1 inch horizontal quartz tube (figure 1.6). Patterned substrates were fabricated using  $O_2$  plasma. First, PDMS/N-Hexane was coated by spin casting on substrates, and PDMS or Glass stamped imprinting (550nm). Then, stamped substrates were exposed by  $O_2$  plasma (figure 2.4). The morphology of the  $VO_2$  nanowires was observed by scanning electron microscopy (SEM). The high-resolution transmission electron microscopy (HRTEM) images were collected using a Cs-corrected JEM-2100 operated at 200keV. The micro-structure of  $VO_2$  nanowires was verified by X-ray Diffraction (XRD) and Raman spectroscopy. Electrical contacts were deposited onto respectively single  $VO_2$  nanowires on the  $SiO_2/Si$  growth substrates. Au/Ti (200/20 nm) electrodes were fabricated by conventional e-beam metal vapor deposition through a metal shadow mask. To minimize contamination, no wet processes were employed at any stage of device fabrication. Current-voltage measurements were done in a custom-built chamber. Samples were annealed in nitrogen for 1minute at 200 °C to improve the Ohmic contact between the nanowire and metallic pads. Metal-to-Insulator transition temperature was measured two-terminal configuration and Raman spectroscopy.

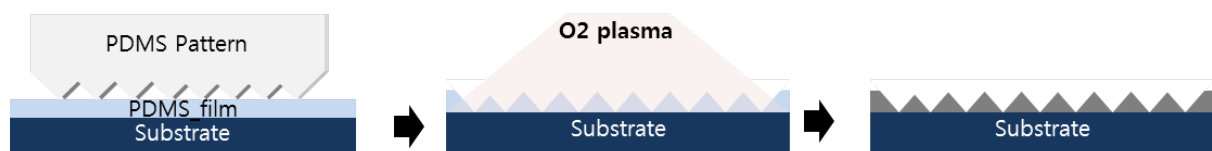


Figure 2.4 Schematic drawing of Patterned substrate process for fabricating the numerous  $VO_2$  nanowire morphologies and the guided growth of millimeter-long  $VO_2$  nanowires.

## 2.2. RESULTS AND DISCUSSION

### 2.2.1. $V_2O_5$ thin film fabrication

To fabricate  $V_2O_5$  thin film, we were deposited with pressure of oxygen and argon. At oxygen partial pressure 10%, the films were seen to be  $V_2O_5$  and  $V_6O_{13}$  and raising oxygen partial pressure 20%,  $V_2O_5$  was observed. Also resistance was increased by hundreds  $M\Omega$  with the rise of the oxygen pressure (Figure 1.6).

Therefore,  $V_2O_5$  thin film was fabricated using a radio-frequency (RF) reactive sputtering chamber with vanadium target (99.99%) and the process conditions are flowing argon (16sccm) /oxygen (4sccm) mixtures under the operating pressure of 4mTorr and substrate temperature of 450°C.

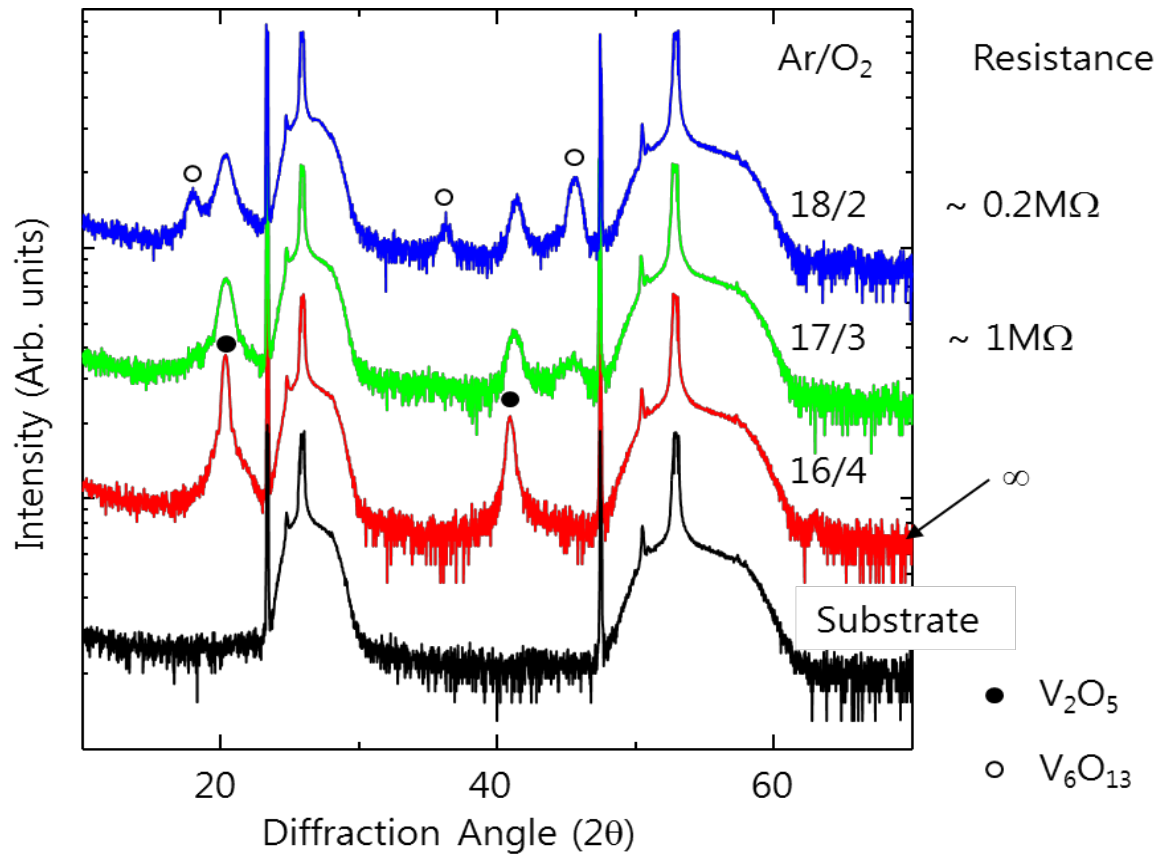


Figure 2.5 The control of  $O_2$  partial pressure led to the formation of  $V_2O_5$  thin film on the sapphire substrate.

### 2.2.2. VO<sub>2</sub> nanowire growth with V<sub>2</sub>O<sub>5</sub> thin film thickness

Respective SEM image show grown VO<sub>2</sub> nanowires on SiO<sub>2</sub> substrates with various thickness of V<sub>2</sub>O<sub>5</sub> thin films from 2 to 20 nm (Figure 2.6). SEM data indicates that 2 min deposition time does not produce nanowires, and many nanoparticles, which were indexed to V<sub>2</sub>O<sub>5</sub>, are observed<sup>[5]</sup> As the deposition time increases to 5 min, the nanowires with quite uniform diameter (of average width of 110nm ( $\pm$  5nm), randomly oriented in the plane of substrate, are found. Figure 2.6 (b) also indicated the presence of  $\sim$  45 nm droplet-like structures around the nanowires, dramatically depleted within about 2 $\mu$ m of the nanowires, showing nanodroplets feeding the growth of the nanowires. Although much more nanowires can be produced at higher thickness of V<sub>2</sub>O<sub>5</sub> thin film, the nanowire widths are too large ( $>$  221 nm) and the width and length uniformity is very poor.

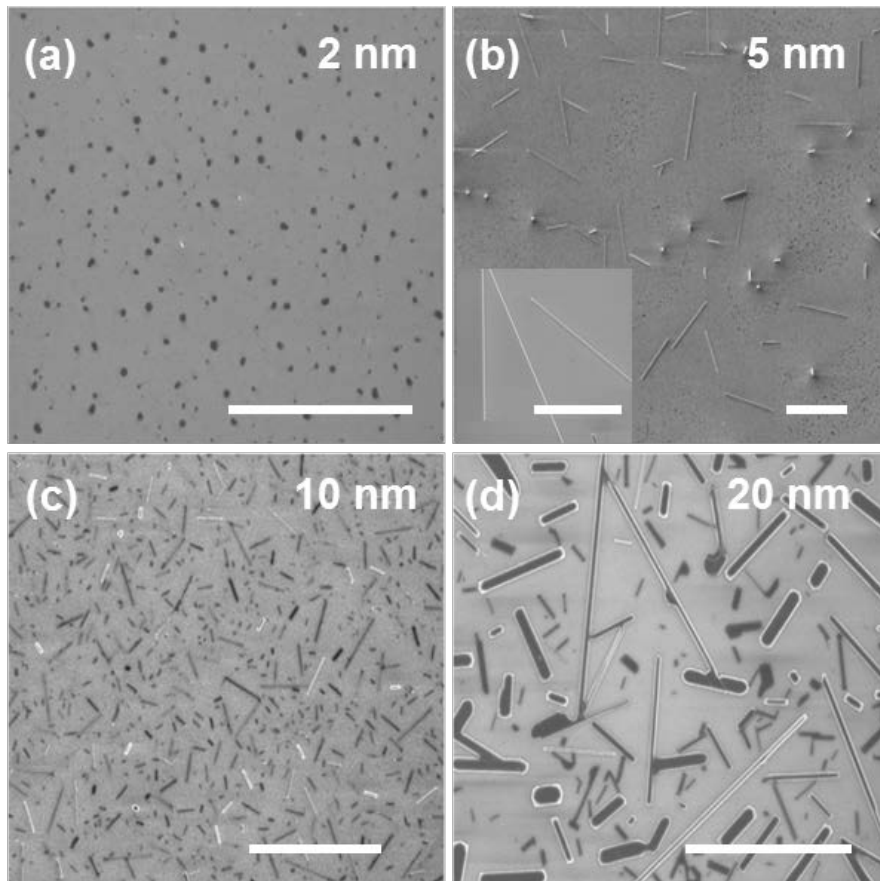


Figure 2.6 SEM images (scale bar = 10  $\mu$ m) of as-grown VO<sub>2</sub> nanowires grown on SiO<sub>2</sub> substrates with varying thickness of V<sub>2</sub>O<sub>5</sub> film from 2 to 20 nm. Inset in (b) shows the representative image of VO<sub>2</sub> nanowires obtained at 5 nm thick-sample.



### 2.2.3. Micro-structure analysis of grown VO<sub>2</sub> nanowires

The nanowires were confirmed by using a high resolution X-ray diffraction (HRXRD) (Figure 2.7a). VO<sub>2</sub> nanowires were grown on a SiO<sub>2</sub>/Si substrate that is lower than the main cure. Only diffraction peaks of (011) and (022) planes are shown, indicating that the VO<sub>2</sub> nanowires synthesize preferential direction.

As excited by 533 nm laser light, Raman spectra of single nanowires is observed (Figure 2.7b). The VO<sub>2</sub> nanowires were grown on a sapphire (Al<sub>2</sub>O<sub>3</sub> c-plane) substrate. The Raman spectra were demonstrated by two peaks at 197 and 225 cm<sup>-1</sup>. To indicate Raman spectra, we retained the laser power of 0.15 mW and had the 300 seconds of exposure time because the VO<sub>2</sub> nanowires is easily deformed and burned from laser-induced heating.

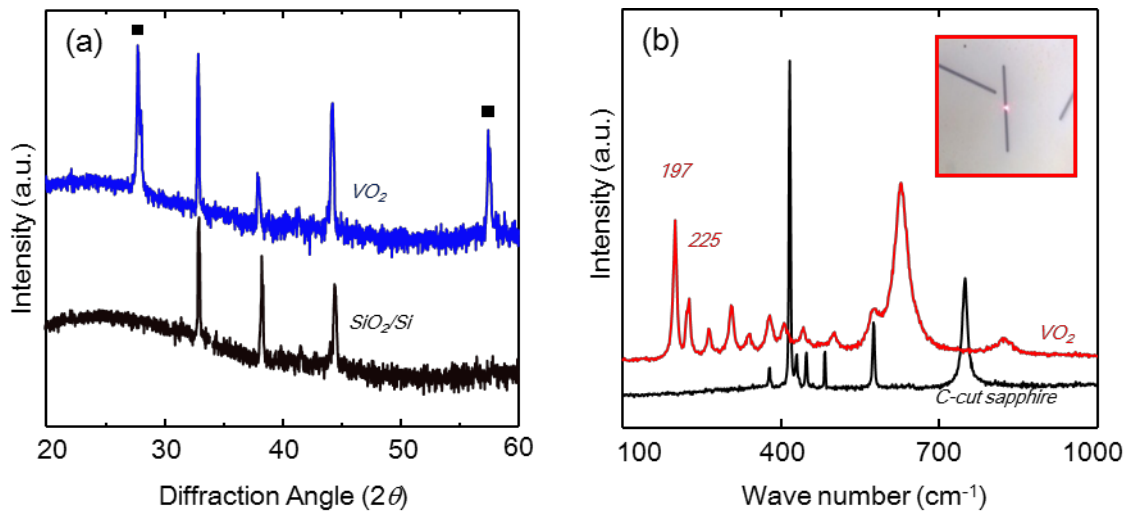


Figure 2.7 (a) XRD diffraction of VO<sub>2</sub> nanowires on a SiO<sub>2</sub>/Si substrate. The VO<sub>2</sub> peaks are observed at the (011) and (022) reflections. (b) Raman spectra of a VO<sub>2</sub> single nanowire on a sapphire substrate. The optical image shows that the laser spot was focused on a VO<sub>2</sub>-nanowire center. Peaks of Raman spectra are shown by sharp peaks at 197 and 225 cm<sup>-1</sup> and broad peak at 630cm<sup>-1</sup>.

#### 2.2.4. Grown VO<sub>2</sub> nanowires with substrates

The VO<sub>2</sub> nanowires were grown by using APPVD with various substrates. Figure 2.8 shows SEM and TEM images of grown VO<sub>2</sub> nanowires on a polished SiO<sub>2</sub>/Si, non-polished SiO<sub>2</sub>/Si and sapphire r-plane. These nanowires synthesized had different directions with substrates. The randomly oriented VO<sub>2</sub> nanowires are located on the polished SiO<sub>2</sub>/Si-substrate bottom. The measured nanowire with was determined by SEM to be 137 ( $\pm$ 34) nm (Figure 2.8a). On a non-polished SiO<sub>2</sub>/Si substrate, the VO<sub>2</sub> nanowires have random angles from a floor (Figure 2.8b). By using r-plane sapphire, VO<sub>2</sub> nanowires were grown to an angle of 60° (Figure 2.8c). TEM was used to characterize the single-crystal structure of a VO<sub>2</sub> nanowire in Figure 2.8 (d), which preferentially grew along the [100] direction in the M1 phase and the atomic images and patterns are also shown as distinct spots clearly, indicating high crystalline properties.

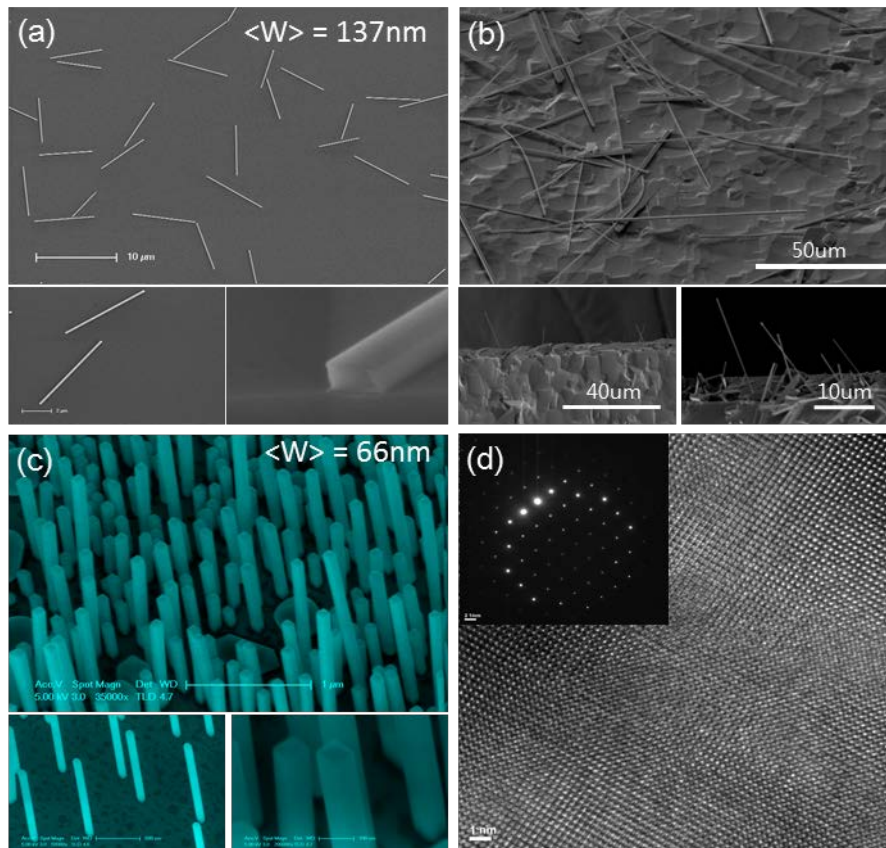


Figure 2.8 (a) Low magnification SEM image of VO<sub>2</sub> nanowires and cross-section image on a polished SiO<sub>2</sub>/Si substrate, (b) The grown VO<sub>2</sub> nanowires on a non-polished SiO<sub>2</sub>/Si substrate, (c) VO<sub>2</sub> nanowires on r-plane sapphire and an angle of 60° from the floor, (d) High magnification TEM images of single VO<sub>2</sub> nanowire.

### 2.2.5. Annealing conditions of metal contact

Au/Ti (200/20 nm) electrodes were deposited onto respectively single VO<sub>2</sub> nanowires on the substrates. The electrodes were fabricated using conventional e-beam metal vapor deposition through a metal shadow mask. In order to minimize contamination, we did not use wet processes at any stage of device fabrication.

We introduced annealing processes to improve the Ohmic contact between the nanowire and metallic pads. Samples were annealed using Rapid Thermal Annealing system (RTA) in a chamber under nitrogen.

Figure 2.9 shows the current change with sweeping the voltage. The current of nA level was observed to 150 °C. At annealing condition of 200°C, we could observe the insulator-to-metal characteristic. The features of nanowires were changed to metallic by annealing VO<sub>2</sub> nanowires at 300 °C. In inserting the optical image, most of the nanowires become nanoparticles over 500 °C. Therefore, we determine the annealing condition at the temperature, 200 °C under nitrogen in a chamber.

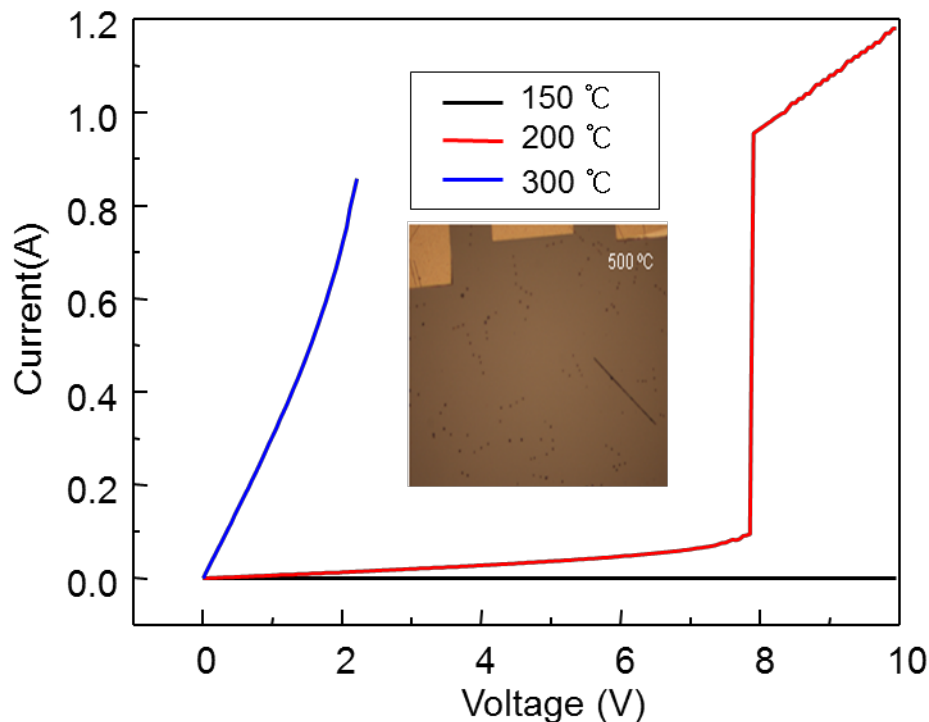


Figure 2.9 Current-voltage curves with the annealing temperatures and VO<sub>2</sub> nanowire condition after an annealing over 500 °C.

## 2.2.6. Calculation of Insulator-to-Metal Transition temperature

All current-voltage measurements were performed in a two-terminal configuration in series with a 10 k $\Omega$  resistor. Previously,<sup>[51]</sup> we suggested that the insulator-to-metal transition temperature could be determined by measuring the voltage values at which the sharp current steps, signaling that occurrence of the insulator-to-metal or the reverse transitions, through the following relationship:

$$V_M^{\uparrow 2} - V_M^{\downarrow 2} \propto (T_M - T_0) \quad (1)$$

The values of TM determined in the above manner as function are shown in Figure 2.10. For the VO<sub>2</sub> nanowire, the Mott transition temperature was found to be  $69.5 \pm 1.2$  °C.

To measure the insulator-to-metal transition temperature, we observed the Raman spectra of a VO<sub>2</sub> single nanowire changing temperatures, heating and cooling the VO<sub>2</sub> nanowire from room temperature to 100°C. Then, the insulator-to-metal transition temperature was obtained by the peak ratio of main peak, 197 cm<sup>-1</sup>.

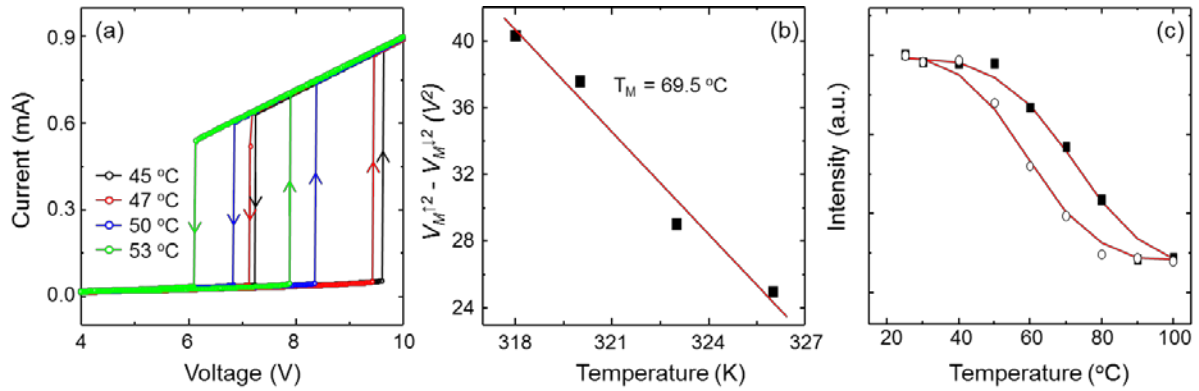


Figure 2.10 (a) I-V curves measured at ambient temperature in the range of 45 - 53 °C by varying the applied bias both from low to high voltage values and in the reverse direction of as-grown VO<sub>2</sub> nanowires, (b) A plot of the difference in the square of the voltages at which the Mott transition occurs in the upward and downward directions vs ambient temperature ( $\Delta V_M^2$  vs T), (c) Heating and cooling temperatures, observed peak ratio of Raman spectra. Raising temperatures, peak of Raman spectra disappeared.

### 2.2.7. Guided growth of sub-millimeter long VO<sub>2</sub> nanowires

The sub-millimeter long VO<sub>2</sub> nanowires were grown using pattern substrates (Figure 2.11). Patterned substrates were fabricated using PDMS/N-Hexane and O<sub>2</sub> plasma. When growing the sub-millimeter long VO<sub>2</sub> nanowires, pattern substrates were located against flowing He gas in an angle of 45° in the middle of a 1 inch horizontal quartz tube furnace.

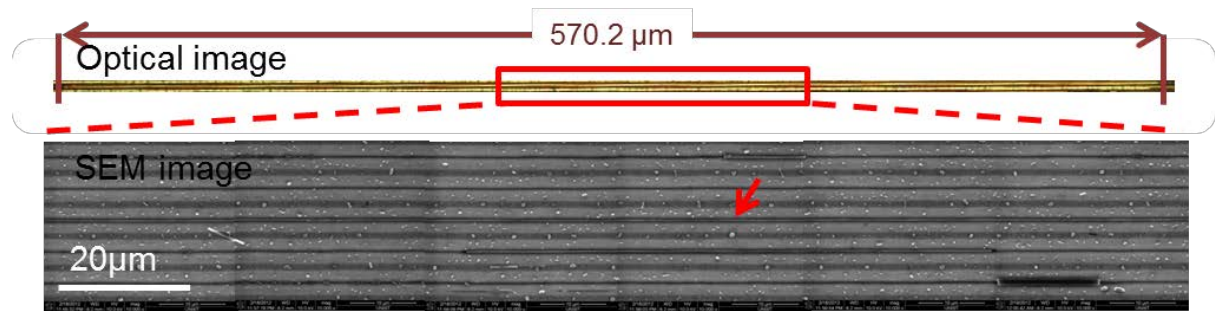


Figure 2.11 Optical and SEM image of sub-millimeter long VO<sub>2</sub> nanowire.

### 2.2.8. VO<sub>2</sub> nanowire morphology control with patterned-substrate shapes

Figure 2.12 shows cross-section SEM image of VO<sub>2</sub> nanowires with controlled morphology. We carried out observation of aligned, sub-millimeter long VO<sub>2</sub> nanowires growth with controlled morphology. Changing the slope of the substrate patterns, we demonstrated that liquid V<sub>2</sub>O<sub>5</sub> nanodroplets coalesce into bigger droplets and large droplets change to VO<sub>2</sub> nanowires. On patterned substrate, the cross-section shapes of VO<sub>2</sub> nanowires are decided by the shapes of bowls. The nanowires are self-aligned and the length can reach to sub-millimeter dimension.

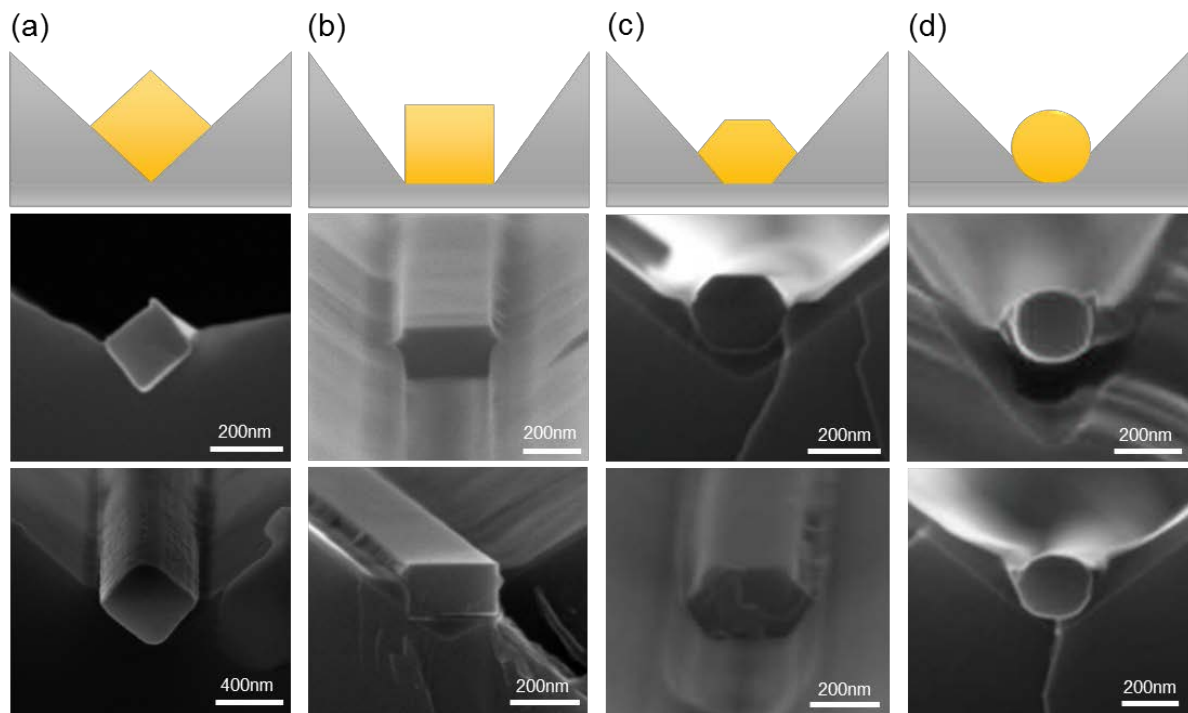


Figure 2.12 The cross-section shapes of VO<sub>2</sub> nanowires, (a) diamond-shaped, (b) rectangular-shaped, (c) hexagonal-shaped, (d) round-shaped. The cross-section shapes of VO<sub>2</sub> nanowires are decided by the shapes of bowls, because the solid V<sub>2</sub>O<sub>5</sub> thin films melt to liquid V<sub>2</sub>O<sub>5</sub> nanodroplets.

### 2.3. CONCLUSIONS

In this summary, we demonstrated the controllable spontaneous conversion of thin films into nanowires for large area production and grew the various VO<sub>2</sub> nanowires with substrates. We used RF reactive sputter for fabricating V<sub>2</sub>O<sub>5</sub> films and single-crystal VO<sub>2</sub> nanowires were grown using physical vapor deposition under atmospheric-pressure. We also verified that sub-millimeter long VO<sub>2</sub> nanowires were synthesized using the patterned substrates. By using various patterned substrates, we could control the VO<sub>2</sub> nanowire morphology. The cross-section morphology of VO<sub>2</sub> nanowires are determined by the shapes of bowls, as the solid V<sub>2</sub>O<sub>5</sub> thin films melt to liquid V<sub>2</sub>O<sub>5</sub> nanodroplets. The insulator-to-metal transition temperature was measured by current-voltage curve and Raman spectra and found to be  $69.5 \pm 1.2$  °C. Due to a number of these features of VO<sub>2</sub> nanowires, they can be used more usefully in devices such as gas and temperature sensors, photovoltaic cells, batteries and so on.

### 3. INTERNAL-STRAIN CREATED BY HYDROGEN GAS IN Pd-VO<sub>2</sub> NEAR COR-SHELL AND APPLICATION AS GAS SENSOR

#### 3.1. EXPERIMENT

##### 3.1.1. Experimental equipment

To deposit the metal contact and Pd nanoparticle, we used E-beam evaporator (Figure 3.1), FC-2000 which is thermal evaporating or e-beam deposition method equipment. Au/Ti (200/20nm) electrodes were fabricated by conventional e-beam metal vapor deposition through a shadow mask. Also, palladium nanoparticles (1 to 3 nm mass thick) were deposited on the device using e-beam evaporation at a very slow deposition rate of less 0.1 Å/s. Electron beam source is shown by the power supply to the hot filament electron beam by the magnetic field induced by magnet. The system is composed of 6 source pocket (Au, Cr, Ni, Ti, Al, Pt, Pd), power supply, 6kW, 208V (CV-6SLZ), source control module, programable sweep controller and Thickness controller.



Figure 3.1 E-beam evaporator, Pd nanoparticle and electrode, Au/Ti (200/20nm) deposition.



For irradiating the electron beam, we used a high voltage electron beam accelerator in Yeungnam University. The nanowires were irradiated with electron beam (e-beam) energy of 0.5 and 0.7 MeV, and doses in range from  $10^{14}$  to  $10^{16}$  electrons/cm<sup>2</sup> at room temperature in ambient conditions. During the irradiation, in order to prevent VO<sub>2</sub> nanowire deformation or damage from induced electron beam heating, we always maintain the beam current of 1mA. The high voltage electron beam accelerator has maximum output 28kW, beam current 40mA, beam energy 0.7 MeV and beam area 1000mm. The system is composed of high frequency converter, capacitance bank, power supply cabinet, SF6 gas supply system, water distributor, shielding room.

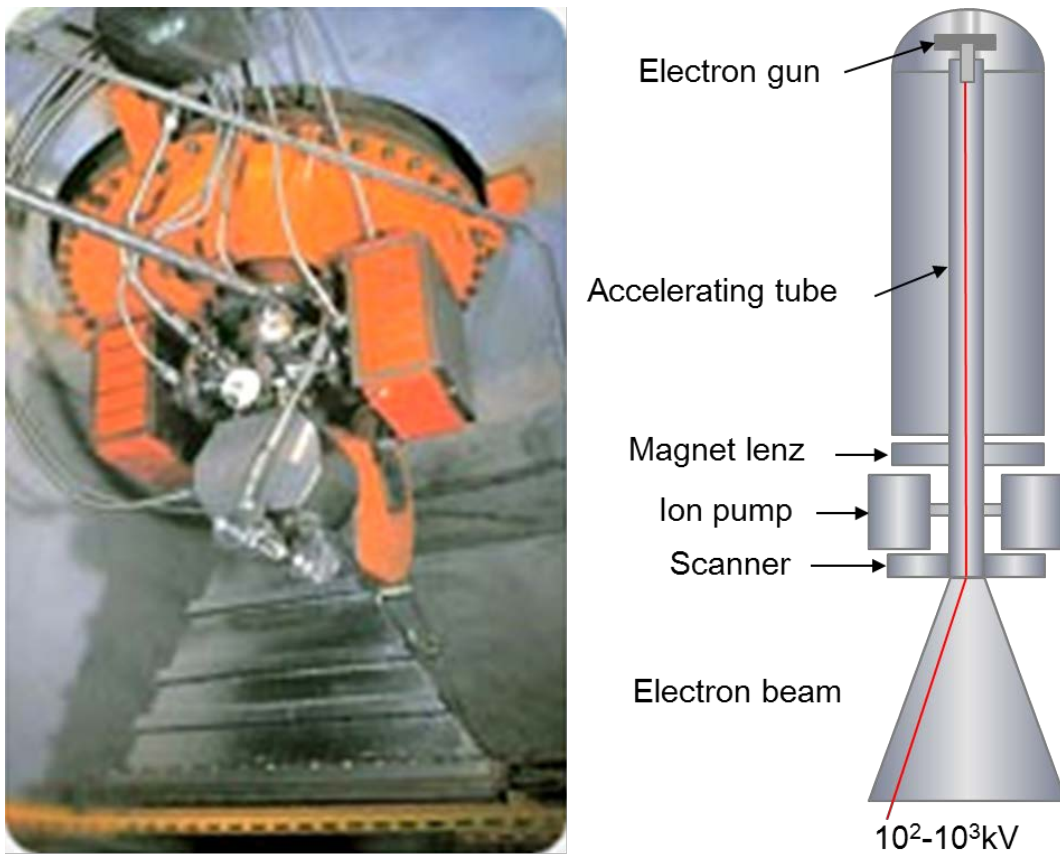


Figure 3.2 Schematic drawing of high voltage electron beam accelerator.

### 3.1.2. Analysis

To detect various gases, the chamber probe station was customized (Figure 3.3). It is possible up to heating 300 °C, pumping 10<sup>-3</sup> torr, and inspecting fore gases. All current-voltage measurements and detecting gases were carried out in a two-terminal configuration in series with a 10 kΩ resistor. The system is composed of a source meter (KEITHLEY 2636A), temperature controller, gas controller, and MFC controller. The source meter offers wide dynamic range from 1fA to 50A and 1μA to 200V. 20,000 rdg/s provides faster test times and ability to capture transient device behavior.

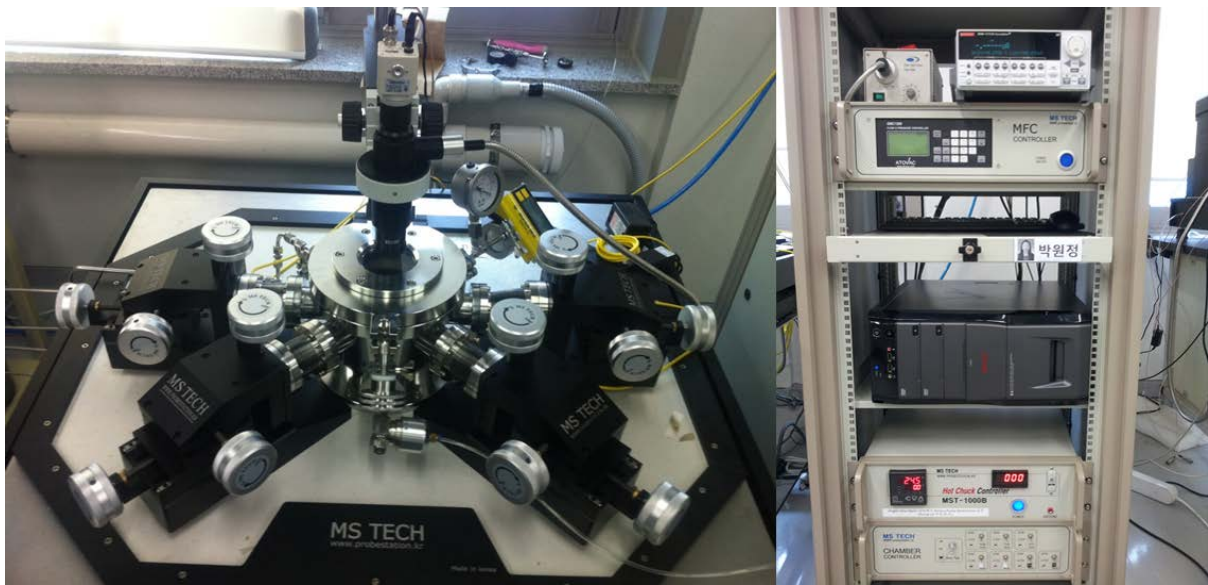


Figure 3.3 Customized current-voltage measurement systems.

### 3.1.3. Experimental methods

To grow the single crystalline vanadium oxide nanowires, the  $V_2O_5$  thin films were initially fabricated onto a thermally grown  $SiO_2$  layer with 2000 Å thickness on a Si (100) single crystal substrate using a radio-frequency (RF) reactive sputtering chamber with a vanadium target of (99.99%), flowing argon (16sccm)/oxygen (4sccm) mixtures under the operating pressure of 4 mtorr and substrate temperature of 450 °C. The  $V_2O_5$  thin films were then transferred into the center of a 1inch horizontal quartz tube furnace to synthesize  $VO_2$  nanowires under atmospheric pressure. The synthesis of  $VO_2$  nanowires was performed during 2hours at 650 °C with flowing high purity He (99.999%) at 300 sccm.

Also, tungsten was deposited with  $V_2O_5$  thin films using a radio-frequency (RF) reactive co-sputtering to fabricate the  $V_2O_5$  thin films doped by tungsten. The nanowires doped by tungsten were carried out for 2hours at 700~750 °C with flowing high purity He(99.999%) at 300 sccm.

The morphology of the  $VO_2$  nanowires was verified by scanning electron microscopy (SEM). The high-resolution transmission electron microscopy (HRTEM) images were collected using a Cs-corrected JEM-2100 operated at 200 kV.

The nanowires were irradiated with electron beam (e-beam) energy of 0.5 and 0.7 MeV, and doses in range from  $10^{14}$  to  $10^{16}$  electrons/cm<sup>2</sup> at room temperature in ambient conditions. During the irradiation, in order to prevent  $VO_2$  nanowire deformation or damage from induced electron beam heating, we always maintain the beam current of 1mA.

Electrical contacts were deposited onto respective  $VO_2$  nanowires on the  $SiO_2/Si$  growth substrates. Au/Ti (200/20 nm) electrodes were fabricated by conventional e-beam metal vapor deposition via a metal-shadow mask. To reduce contamination, no wet processes were employed at any stage of device fabrication and then, we introduced annealing processes to improve the Ohmic contact between the nanowire and metallic pads. Samples were annealed using Rapid Thermal Annealing system (RTA) in a chamber under nitrogen. After the fabrication of single- $VO_2$  nanowire device, palladium nanoparticles (1 to 3 nm mas thick) were deposited on the device using e-beam evaporator at a very slow deposition rate of less 0.1Å/s. In carrying out Pd deposition, a shadow mask was appropriately placed so that each device set contained both pristine and Pd-decorated  $VO_2$  nanowires samples.

Finally, all samples were annealed in a nitrogen atmosphere for 1 min at 100 ~ 200 °C to induce the palladium metal film to break up and aggregate into well-spaced Pd nanoparticles. Current-voltage measurements were done in a custom-built chamber in which the temperature and gas composition could be varied. Ambient gas composition was controlled by mass flow meters and gas partial pressures were in the range 10- 100 Torr.

To observe the effect of  $VO_2$  nanowire stress,  $VO_2$ nanowires were grown on non-polishing  $SiO_2$

substrate for transfer of the nanowires. Substrates of flexible devices were used by the polyimide film. For catching the VO<sub>2</sub> nanowire, Au/Ti (400/10 nm) electrodes were fabricated by conventional e-beam metal vapor deposition via a metal-shadow mask.

## 3.2. RESULTS AND DISCUSSION

### 3.2.1. VO<sub>2</sub> nanowires doped by tungsten

Tungsten was doped into the V<sub>2</sub>O<sub>5</sub> thin films. When we fabricated the V<sub>2</sub>O<sub>5</sub> thin films, tungsten was doped using a radio-frequency (RF) reactive sputtering chamber with a tungsten target of (99.99%), flowing argon (16sccm)/oxygen (4sccm) mixtures under the operating pressure of 4 mtorr. First, we made plasma to the tungsten gun, flowing argon (16sccm)/oxygen (4sccm) mixtures under the operating power 5W. Then, the vanadium gun was opened for co-sputtering.

VO<sub>2</sub> nanowires doped by tungsten were grown by atmospheric pressure, physical vapor deposition during 2hours at 700~750 °C with flowing high purity He(99.999%) at 300 sccm.

Figure 3.4 shows the VO<sub>2</sub> nanowires doped by tungsten. The W-doped VO<sub>2</sub> nanowires indicated that the both ends of nanowires show a little change.

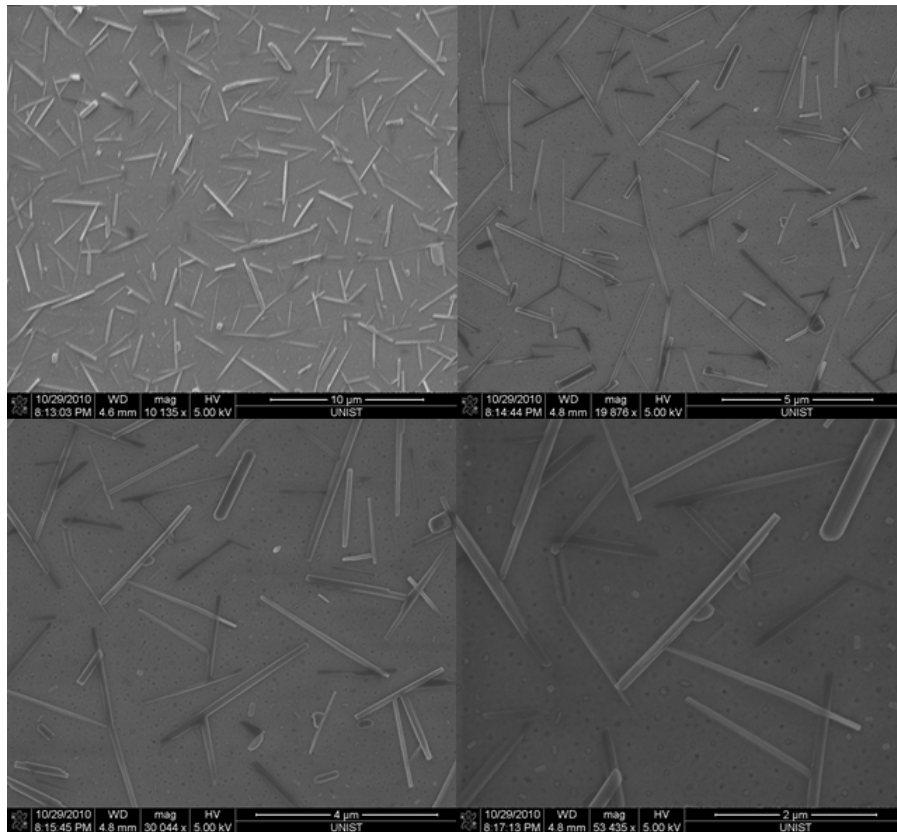


Figure 3.4 SEM images of VO<sub>2</sub> nanowires doped by tungsten.

### 3.2.2. Analysis of VO<sub>2</sub> nanowires doped by tungsten

Following the doping tungsten, the Raman spectra remain unchanged (Figure 3.5a). Recent study reported that Mott transition temperature is to be reduced as doping other atoms into vanadium dioxide.<sup>[52]</sup> Figure 3.5b shows that by doping tungsten into the VO<sub>2</sub> nanowires, insulator-to-metal transition temperature was reduced to 35°C. Energy dispersive x-ray spectroscopy indicated that tungsten is doped into VO<sub>2</sub> nanowires (Figure 3.5c).

To measure the Mott transition temperature, we inspected the Raman spectra of a VO<sub>2</sub> single nanowire changing temperatures, heating the nanowire from room temperature to 55°C. Then, the insulator-to-metal transition temperature was obtained by the peak ratio of main peak, 197 cm<sup>-1</sup>.

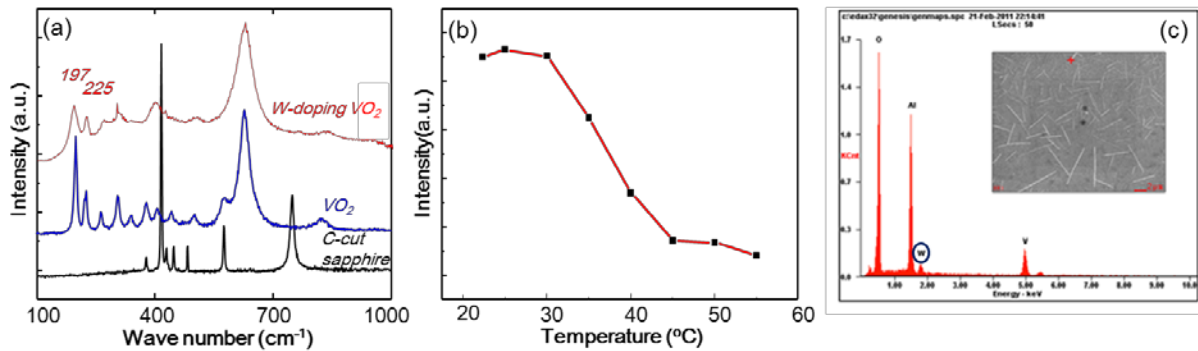


Figure 3.5 (a) substrate and VO<sub>2</sub> nanowire and W-doped VO<sub>2</sub> nanowire of Raman spectra, (b) Heating temperatures, observed peak ratio of Raman spectra. Raising temperatures, peak of Raman spectra disappeared, (c) 2.5% W-doped EDX result.

### 3.2.3. Current-density change with e-beam irradiation conditions

All  $I$ - $V$  measurements were carried out in a two-terminal configuration in series with a  $10\text{ k}\Omega$  resistor. We monitored the irradiation effects as a function of irradiation energy and dose (Figure. 3.6). For the as-grown  $\text{VO}_2$  nanowire, the current increased linearly with increasing voltage with a slope corresponding to a conductance value of  $1.50 \times 10^{-6}\ \Omega^{-1}$ . The conductance value increased to  $3.57 \times 10^{-6}\ \Omega^{-1}$  as the dose (at  $0.5\text{ MeV}$ ) increased to  $10^{16}/\text{cm}^2$  and  $I$ - $V$  curve became slightly steep with the voltage. The increase in the irradiation energy to  $0.7\text{ MeV}$  also increased further the conductivity by about twice, measured at  $5\text{ V}$ . The significant increase in the conductivity may be due to the local composition deviations in material stoichiometry such as oxygen vacancies by the e-beam irradiation. Actually, a large amount of vacancies can be generated during the e-beam irradiation. Some deep levels or midgaps formed by oxygen vacancies or disorder effects may play an important role in increasing the conductivity.<sup>[53]</sup> The variation of current density with the e-beam irradiation is plotted after measuring the electrical properties of several nanowires in Figure 3.6(b).

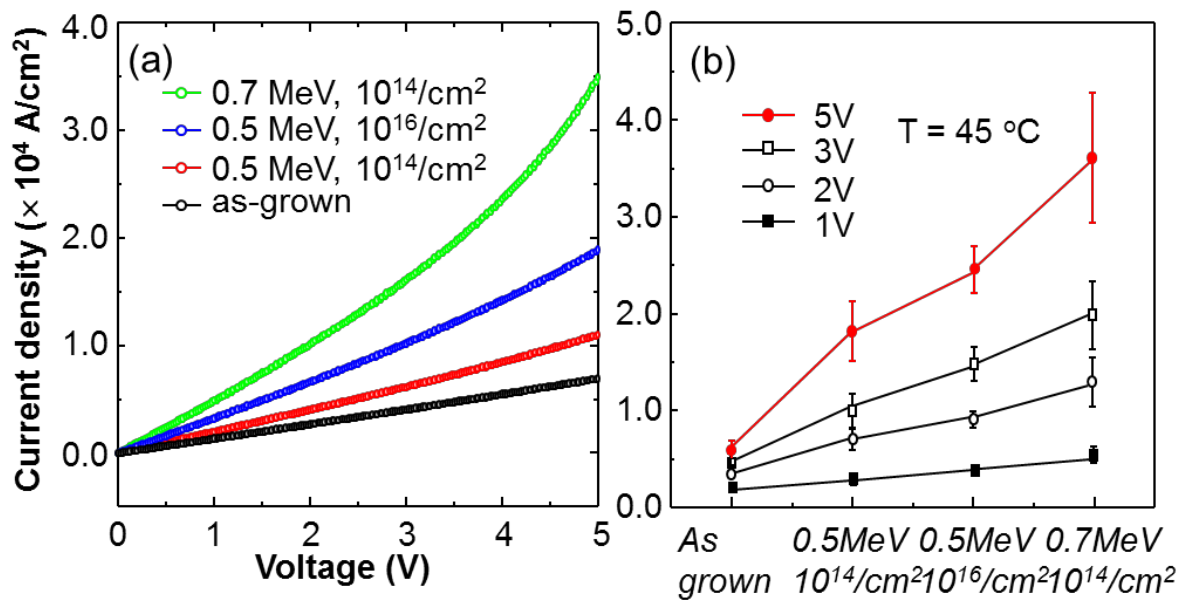


Figure 3.6 Change in current density of  $\text{VO}_2$  nanowires as a function of e-beam irradiation power and dose.

### 3.2.4. Crystal structure analysis of VO<sub>2</sub> nanowires following e-beam irradiation

The crystal structures of the VO<sub>2</sub> nanowires after e-beam irradiation were characterized by HR-TEM images and the corresponding fast Fourier transform (FFT) patterns, as shown in Figure 3.7. Previously,<sup>[51]</sup> we showed that only diffraction peaks corresponding to (011) and (022) planes were observed, indicating that the VO<sub>2</sub> nanowires grow along a preferential direction. In TEM image of the as-grown VO<sub>2</sub> nanowire, the atomic images and patterns are also shown as distinct spots clearly, indicating high crystalline properties. After e-beam irradiation of 0.5 MeV at dose of 10<sup>16</sup>/cm<sup>2</sup>, the atomic images remain unchanged although the diffraction spots look a little larger. Even after e-beam irradiation of 0.7 MeV, it cannot easily be seen that the lattice image is distorted. However, the diffraction spots became larger and were split into several smaller spots, suggesting deterioration in the crystalline properties of the material. Nevertheless, it should be noted that any secondary phases such as V<sub>2</sub>O<sub>5</sub> were not produced.

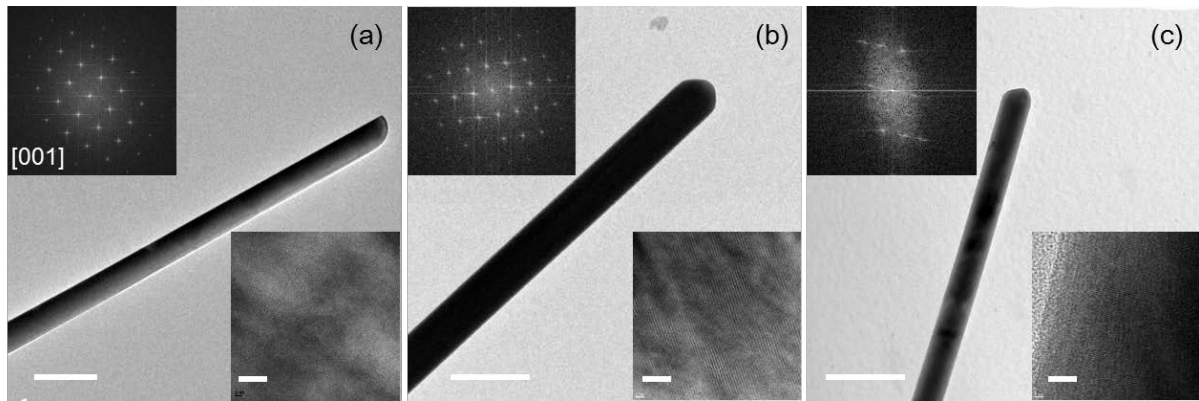


Figure 3.7 Bright-field images (scale bar = 100 nm), and HR-TEM images (scale bar = 5 nm), and the corresponding Fast Fourier Transformed (FFT) diffraction patterns of VO<sub>2</sub> nanowires as a function of e-beam irradiation power and dose; (a) as-grown (b) 0.5 MeV, 10<sup>16</sup>/cm<sup>2</sup> (c) 0.7 MeV, 10<sup>14</sup>/cm<sup>2</sup>.



### 3.2.5. Mott transition temperatures with e-beam irradiations; I-V measurement

Previously,<sup>[51]</sup> we suggested that the insulator-to-metal transition temperature could be determined by measuring the voltage values at which the sharp current steps, signaling that the occurrence of the insulator-to-metal or the reverse transitions, through the relationship;

$$V_M^{\uparrow 2} - V_M^{\downarrow 2} \propto (T_M - T_0) \quad (1)$$

The values of  $T_M$  determined in the above manner as a function of irradiation energy and dose are shown in Figure 3.8. For the as-grown  $\text{VO}_2$  nanowire, the Mott transition temperature was found to be  $69.5 \pm 1.2$  °C. With e-beam irradiations, the measured values of  $T_M$  ranged from 68.8 to 73.3 °C, depending the energy and dose, within the experimental error ( $\pm 2$  °C) inherent in the determination of  $T_M$ , meaning that the effect of e-beam irradiation is negligible.

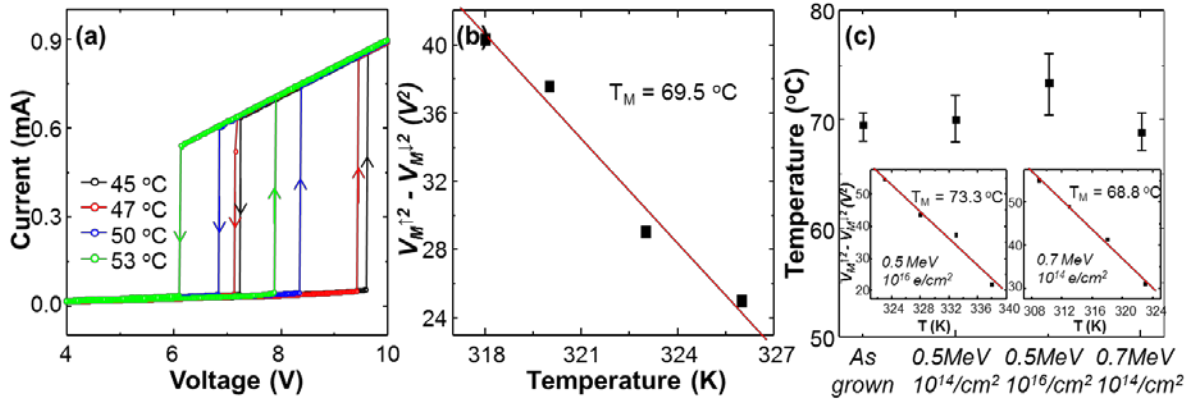


Figure 3.8 (a) I-V curves measured at ambient temperature in the range of 45 - 53 °C by varying the applied bias both from low to high voltage values and in the reverse direction of as-grown  $\text{VO}_2$  nanowires, (b) A plot of the difference in the square of the voltages at which the Mott transition occurs in the upward and downward directions vs ambient temperature ( $\Delta V_M^2$  vs T), (c) The Mott transition temperatures as a function of e-beam irradiation energy and dose (inset) A plot of the difference in the square of the Voltages after e-beam irradiation of 0.5 MeV at dose of  $10^{16}/\text{cm}^2$  and after e-beam irradiation of 0.7 MeV at dose of  $10^{14}/\text{cm}^2$ .

### 3.2.6. Mott transition temperatures with e-beam irradiations; Raman Spectra

Raman spectra of a single VO<sub>2</sub> nanowire on sapphire (c-plane) excited by 523nm laser light. Raman spectra indicated the two characteristic peaks at 197 and 225 cm<sup>-1</sup> which are attributable to single crystal monoclinic VO<sub>2</sub>. By heating and cooling a VO<sub>2</sub> nanowire from room temperature to 100 °C, the insulator-to-metal transition temperature was obtained by the peak ratio of first main peak, 197 cm<sup>-1</sup>. There is little change in insulator-to-metal transition temperature under convergent electron beam irradiation at 0.5 and 0.7MeV.

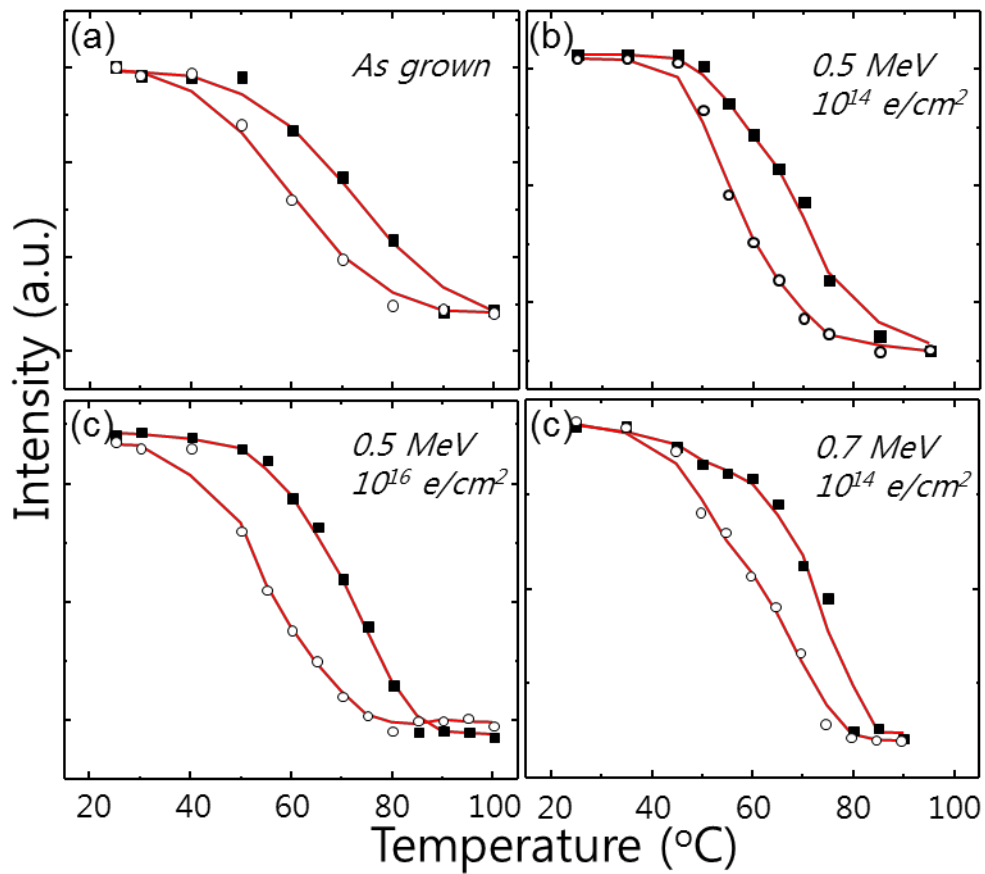


Figure 3.9 Mott transition temperatures with irradiation conditions. Raman peak (197 cm<sup>-1</sup>) was observed by heating and cooling a VO<sub>2</sub> nanowire.

### 3.2.7. Sensing performance with e-beam irradiation conditions

Figure 3.10 (a) shows a typical current response measured at constant voltage of Pd-decorated VO<sub>2</sub> nanowire obtained at 45 °C, exposed to hydrogen flowing at 10 sccm added for various lengths of time to a 100 sccm background air stream. Initiating the hydrogen flow across a Pd-decorated VO<sub>2</sub> nanowire biased at 5 V causes the current to increase steadily and then increase approximately 1000-fold after ~10 min of H<sub>2</sub>. Thus, the electrical conductance of the VO<sub>2</sub> nanowire is found to change over two time scales: a slow process taking place over several minutes depending on the conductivity and ambient temperature, and an ultra-fast process which takes a few nano- or micro-seconds to reach the metallic phase. Previously,<sup>[6]</sup> we argued that the slow process was complex, in addition to H atom formation and its interaction with the Pd, such as H atom migration into the oxide's surface and its penetration into the oxide's bulk region, known as spillover effect.

Figure 3.10 (b) shows the sensing performance of Pd-decorated VO<sub>2</sub> nanowire as a function of irradiation energy and dose. After e-beam irradiation of 0.5 MeV at a dose of 10<sup>14</sup>/cm<sup>2</sup>, the response time slightly decreases to an average of 7 (± 2) min. When the dose increases to 10<sup>16</sup>/cm<sup>2</sup>, the response time (< 4 min) significantly reduces to less than half of initial values (~ 10 min). This acceleration in hydrogen response may be considered as the result of the increase of nanowire temperature due to Joule self-heating.<sup>[54, 55]</sup>

In Figure 3.10 (b), turning on the hydrogen flow before e-beam irradiation causes the current to increase very slowly and then the rate of increase in current significantly increases after ~ 7 min of H<sub>2</sub> exposure. After e-beam irradiation of 0.5 MeV at dose of 10<sup>16</sup>/cm<sup>2</sup>, the rate already begins to increase significantly after only 1~2 min of H<sub>2</sub> exposure. As mentioned above, the increase in the current is due to the increase of electron concentration by the hydrogen interstitials. However, the supply of electrons to VO<sub>2</sub> due to the reaction between Pd nanoparticles and hydrogen atoms is not likely enough for accelerating the MIT. Actually, it takes several minutes (~ 5 min) for the device current of as-grown VO<sub>2</sub> nanowire to reach the initial value of e-beam-irradiated nanowire (0.5 MeV at dose of 10<sup>16</sup>/cm<sup>2</sup>). The significant increase of the rate of increase in current after several minutes of H<sub>2</sub> exposure (depending on the conductivity) may be ascribed to Joule self-heating due to the further increase in electron concentration. All *I-V* measurements in Figure 3.10 (b) show that the MIT is triggered at threshold current of approximately 1~3 × 10<sup>-5</sup>A although the irradiated nanowires show higher threshold current than that of an as-grown nanowire.

The change in the response time of Pd-decorated VO<sub>2</sub> nanowires with e-beam irradiation is summarized in Figure 3.10 (c). Interestingly, the response time drastically decreased to less than 10 sec as the Pd thickness increased to 2.5 nm. Some of them are found to have fast response characteristics of 1~2 sec. For the devices showing such a fast response time, the response behavior is totally

different, compared with the devices showing slow response. These aspects, which are currently being investigated, will be the subject of a separate publication.

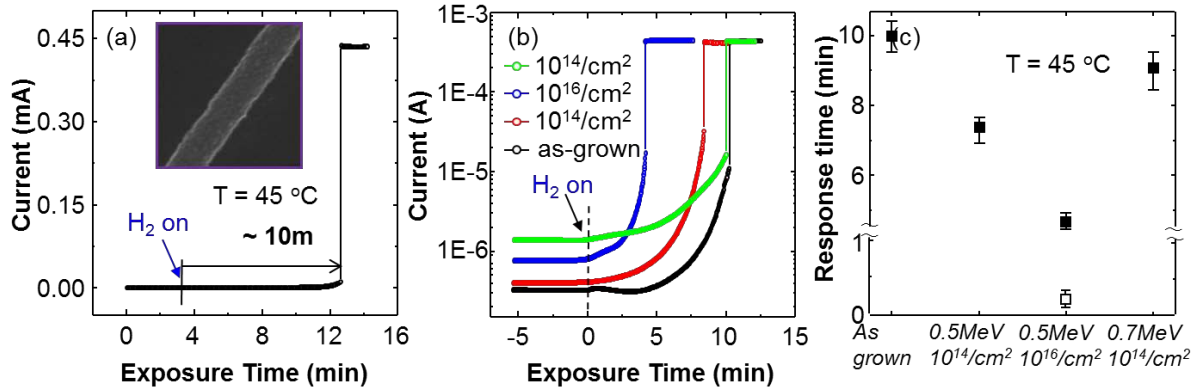


Figure 3.10 (a) The change in current for a Pd-decorated as-grown  $\text{VO}_2$  nanowire biased at 10 V as a function of time of exposure to hydrogen gas, (b) The change in current as a function of e-beam irradiation energy (0.5 MeV: red and blue curves, 0.7 MeV: green curve) and dose, (c) The response time as a function of e-beam irradiation energy. The open square is a result of response time measured when the Pd thickness is increased to 2.5 nm.

### 3.2.8. Detecting hydrogen gas at the room temperature

This reduction in the response time due to the increase of the conductivity could be observed near room temperature (35 ~ 40 °C), as shown in Figure 3.11. After e-beam irradiation of 0.5 MeV at dose of  $10^{14}/\text{cm}^2$ , it takes tens of minutes (> 10 min) for the insulator to metal transition at 40 °C. However, when the dose increases to  $10^{16}/\text{cm}^2$ , the response time significantly decreases to less than 4 min. When it is measured at 35 °C, the hydrogen induces the MIT within 6 ~ 7 min. Thus, the increase in conductivity can be an effective method in improving the sensing performance and may make it useful at ambient room temperature or lower.

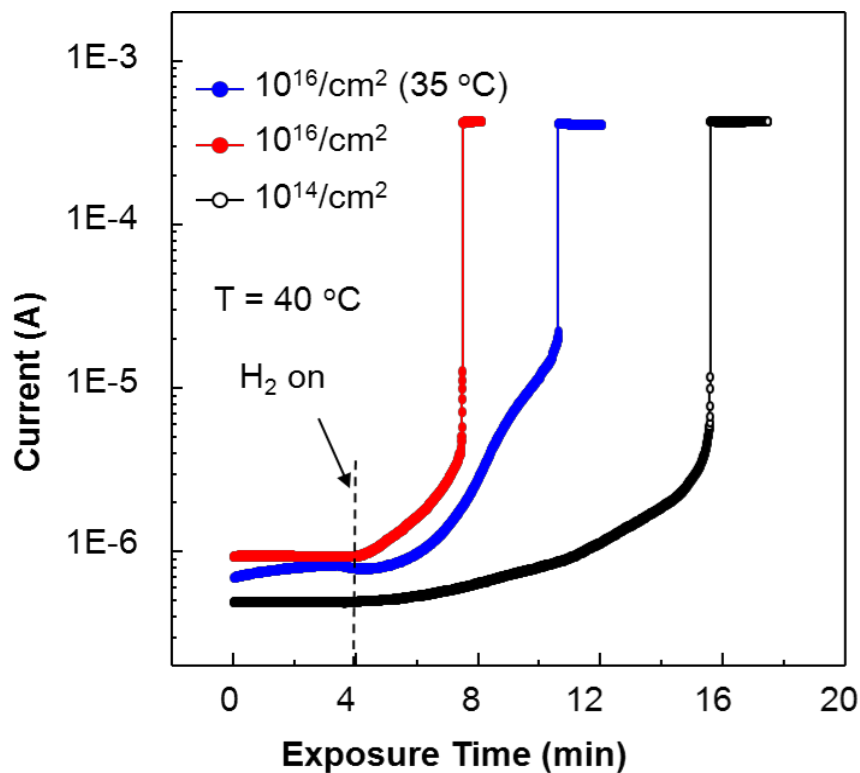


Figure 3.11 The change in current for a Pd-decorated as-grown  $\text{VO}_2$  nanowire biased at 10 V as a function of time of exposure to hydrogen gas with e-beam irradiation energy and dose, measured at 35 °C and 40 °C.

### 3.2.9. The selectivity of different four gases

More noteworthy is the observation that Pd-decorated VO<sub>2</sub> nanowire is very effective in detecting only hydrogen gas. Figure 3.12 shows the change in sensitivity for several gases; hydrogen, oxygen, carbon monoxide, and ethylene. Of all gases, significant change in current is observed with only hydrogen and turning on the other gases flow (10 sccm) produced  $\leq 10\%$  changes (the change in current with CO flow is plotted in the inset). This may tell us that if catalytic nanoparticles interacting strongly with specific gases are designed with optimization and properly decorated onto VO<sub>2</sub> nanowires, such ultra-sensitive gas response can be obtained selectively at low temperature.

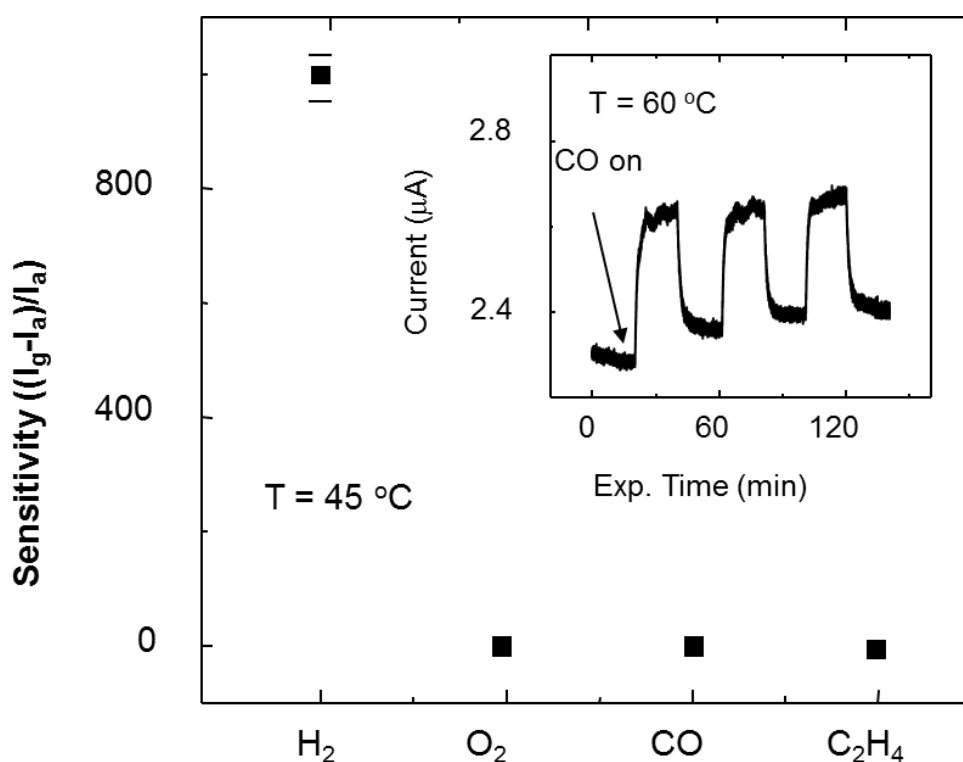


Figure 3.12 The selectivity of sensors in detecting hydrogen gas of different four gases (H<sub>2</sub>, O<sub>2</sub>, CO, and ethylene). Inset shows the CO response measured at 60 °C.

### 3.2.10. The temperature coefficient of resistance

The actual mean temperature of the nanowire can be accurately measured using the resistance of the nanowire itself as the temperature was varied from 303 K to 323 K in the presence of hydrogen (Figure 3.13). From the data, a temperature coefficient of resistance,  $\alpha = 2.30 \pm 0.02 \times 10^{-2} \text{ K}^{-1}$  was obtained, confirming results presented in the literature.<sup>[56]</sup>

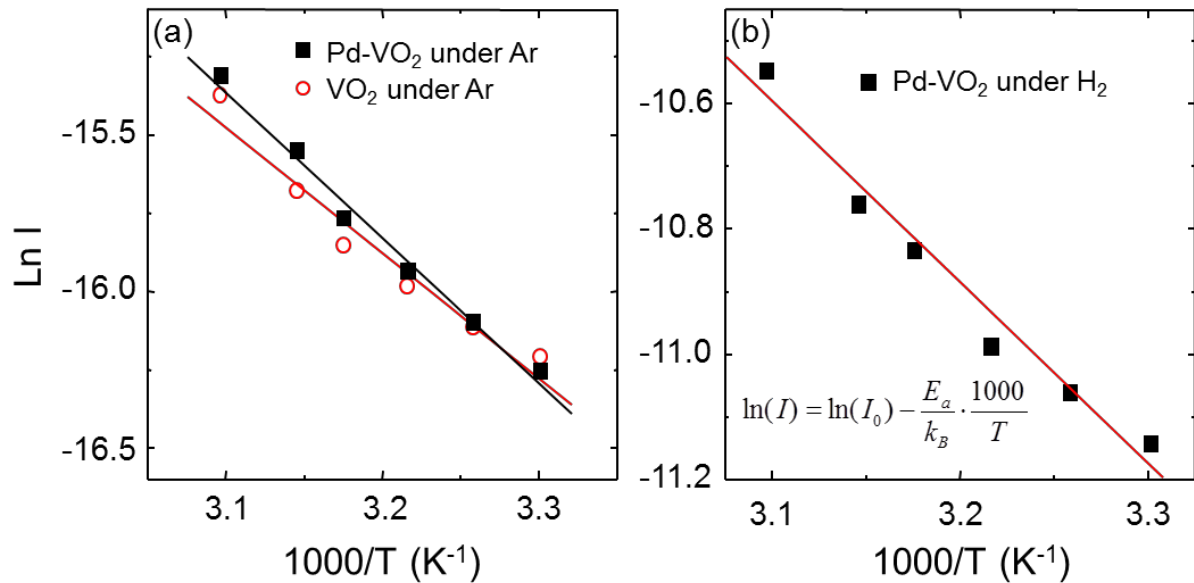


Figure 3.13 Plots of  $\ln I$  vs.  $100/T$  of  $\text{VO}_2$  under Ar,  $\text{Pd-VO}_2$  under ar and  $\text{H}_2$ .

### 3.2.11. VO<sub>2</sub> nanowire temperature calculation by COMSOL multiphysics package

We conducted finite element simulations using a COMSOL multiphysics package (Version 4.2) in order to find the final temperature of a VO<sub>2</sub> nanowire due to Joule heating. In our model, a VO<sub>2</sub> nanowire of which both ends are connected by two Au electrodes is supported by a SiO<sub>2</sub> substrate. We apply a 5 V external voltage at the ends of Au electrodes and keep the temperature to the ambient temperature. The heat generated in the VO<sub>2</sub> nanowire due to the applied voltage transfers to the SiO<sub>2</sub> substrate and Au electrodes by conduction and to air by free convection. The detail dimension, condition and material constants are given in **Table 1**. The resulting temperature-versus-distance plots reveal that within 20 μm of the electrical contacts, the actual temperature of the nanowire increases from 0.163 °C to 1.137 °C as the conductance increases (Figure 3.14). Thus, Joule self-heating may not enough for accelerating the MIT and so the effect can be negligible.

At these current values at which the MIT is triggered (Figure 3.10b), the nanowire temperature could be calculated to be in the range of 53 ~ 64 °C, a little lower than most reported values (~ 68 °C) of MIT (Figure 3.14). The slight decrease of nanowire temperature at transition ( $\Delta T = 4 \sim 13$  °C) is thought to be due to the increase in the electron concentration, considered as Mott-Hubbard type, although the competing roles of electron-phonon and electron-electron coupling to the structural and electronic properties of VO<sub>2</sub> are still unclear and of an active area.<sup>[19, 57]</sup>

**Table 1** Dimension, electrical and thermal conductivity of VO<sub>2</sub> nanowire and SiO<sub>2</sub> substrate.

VO <sub>2</sub> nanowire dimension W x H x L [μm]	0.1 x 0.07 x 20.0
SiO <sub>2</sub> substrate dimension W x H x L [μm]	100 x 100 x 100
Current density of nanowire J [A/cm <sup>2</sup> ]	0.5 x 10 <sup>4</sup> , 1.0 x 10 <sup>4</sup> , 3.5 x 10 <sup>4</sup>
Thermal conductivity of nanowire K <sub>n</sub> [W/(m·K)]	5.10
Thermal conductivity of nanowire K <sub>s</sub> [W/(m·K)]	1.05
Applied voltage E <sub>app</sub> [V]	5.0
Ambient and Initial Temperatures [°C]	45.0



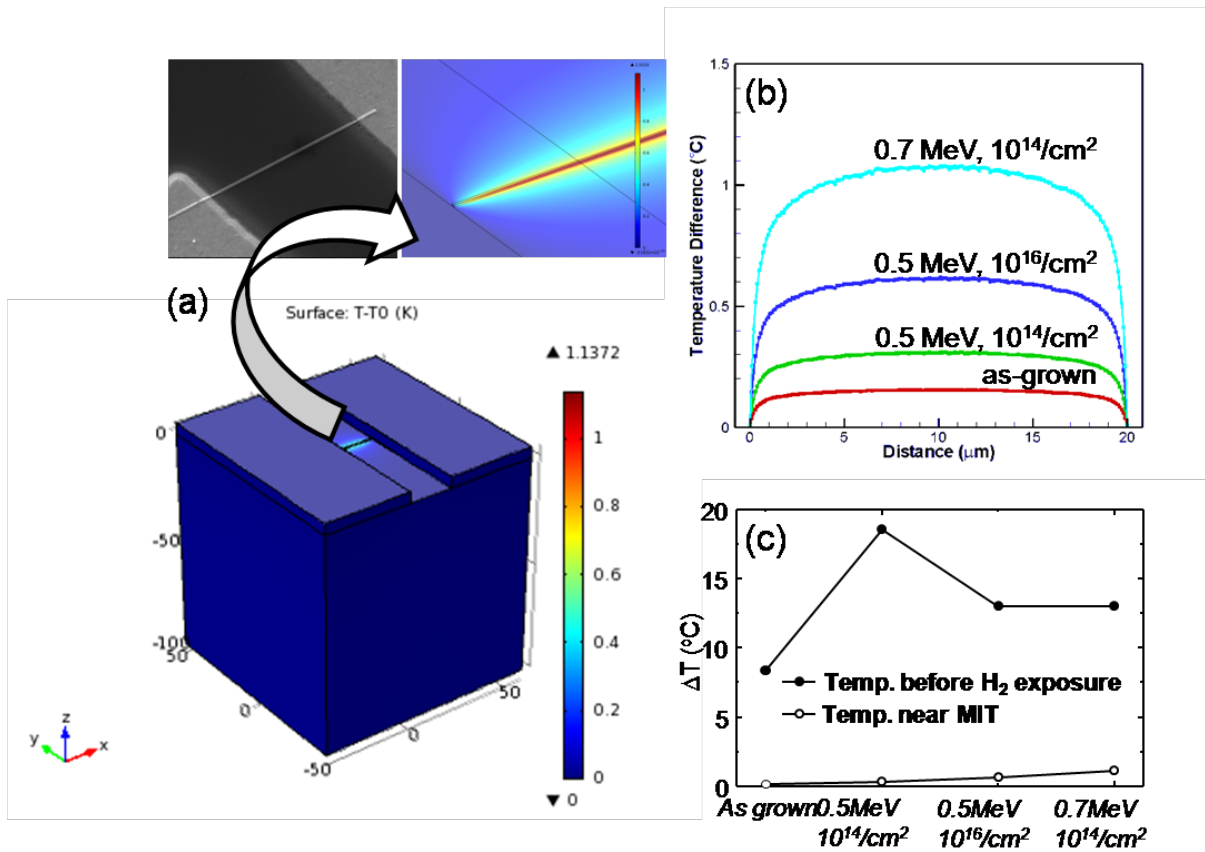


Figure 3.14 (a) 3D model in COMSOL of a VO<sub>2</sub> nanowire (lateral dimension: 70x 100 nm) on a SiO<sub>2</sub>/Si substrate (Inset shows the SEM image of the VO<sub>2</sub> nanowire), (b) Plots of  $\Delta T$  versus distance along the axis of the nanowire shown in (a) measured at 5V as a function of e-beam irradiation power and dose. (c) temperature difference of nanowires before H<sub>2</sub> exposure and near MIT as a function of e-beam irradiation power and dose.

### 3.2.12. Induced defects from high e-beam energy

The formation of structural defects such as oxygen vacancies may also be responsible for such a fast response time because the defects can elevate atomic hydrogen diffusion into  $\text{VO}_2$ . However, increasing the e-beam energy to 0.7 MeV does not reduce the response time to the initial value of non-irradiated nanowire although the conductivity increases up to about 7 times, compared with as-grown  $\text{VO}_2$  nanowire. This may likely be due to the structural disorder that degrades its switching efficiency and hysteresis behavior. In fact, most of them were broken before the transition occurs, meaning that higher e-beam energy reduces the stabilization of the crystal. (Figure 3.15)

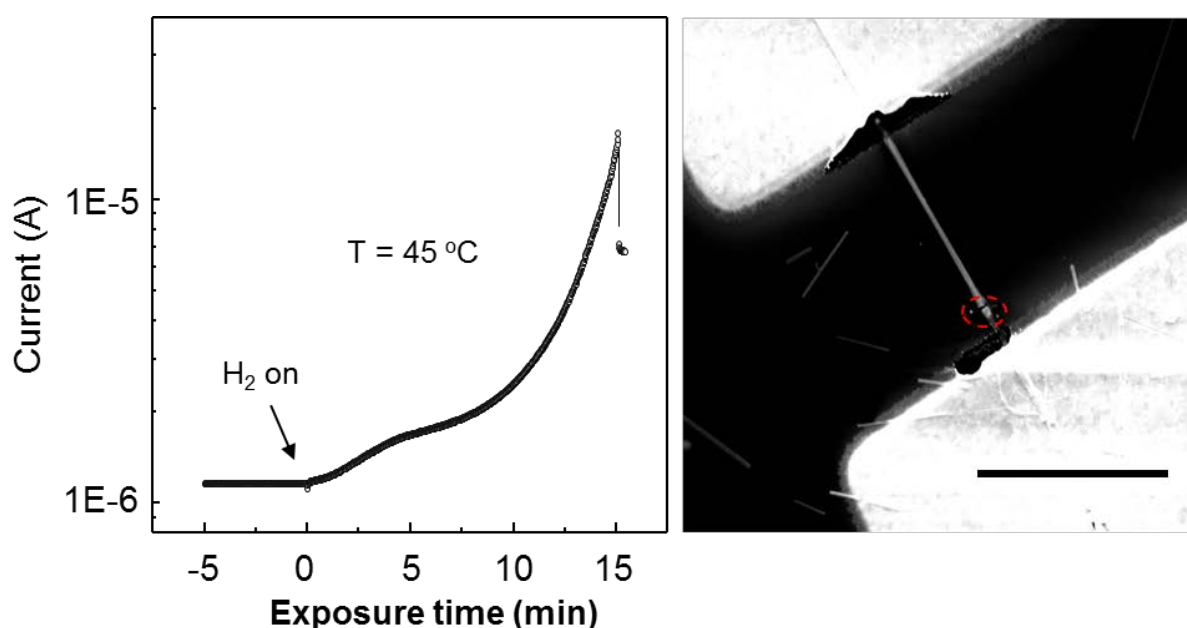


Figure 3.15 I-V curve and SEM image of Pd- $\text{VO}_2$  after e-beam irradiation at 0.7 MeV. This information is available free of charge via the Internet at <http://pubs.acs.org>.

### 3.2.13. SEM & TEM images of palladium deposited & non-deposited VO<sub>2</sub> nanowires

Figure 3.16 shows the typical nanowire with the length around several hundred micrometers and the thickness around of 200 nm, which can be tuned by adjusting the growth conditions. Transmission electron microscopy (TEM) was used to characterize the single-crystal structure of a VO<sub>2</sub> nanowire in Figures 3.16 (b) and 3.16 (c), which preferentially grew along the [100] direction in the M<sub>1</sub> phase and the atomic images and patterns are also shown as distinct spots clearly, indicating high crystalline properties. SEM images (Figures 3.16e and 3.16f) indicate that the diameters of the palladium nanoparticles were in the range of 5-15 nm and the distance between the nanoparticles were in the range of 3-10 nm depending on the mass thick.

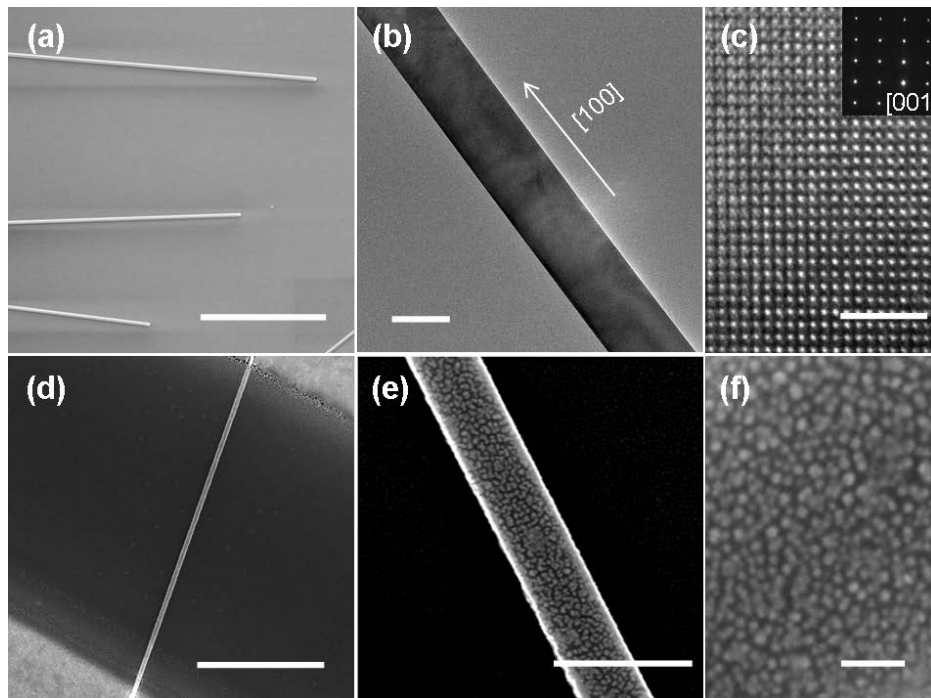


Figure 3.16 (a) Low magnification SEM image of VO<sub>2</sub> nanowires, (b) Low magnification and (c) high magnification TEM images of single VO<sub>2</sub> nanowire, (d) SEM image of single nanowire spanning gold contacts separated by about 15  $\mu\text{m}$ . Low magnification, (e) and high magnification (f) SEM images of Pd-decorated single VO<sub>2</sub> nanowire. The scale bar is 10  $\mu\text{m}$ , 200 nm, 2 nm, 100 nm, 5  $\mu\text{m}$ , and 500 nm respectively.

### 3.2.14. Response rate with palladium thickness

Most of the I-V curves were carried out in a two-terminal configuration in series with a 10k $\Omega$  resistor and at ambient temperatures of 50 °C, with Pd nanoparticles decorating the surface of the nanowires. Figure 3.17 shows a current response measured at constant voltage and plotted in semi-log scale of Pd-decorated VO<sub>2</sub> nanowire, exposed to hydrogen flowing at 5 sccm added for various lengths of time to a 1000 sccm background air stream with Pd thickness. When 1 nm Pd was deposited and annealed, initiating the hydrogen flow across a Pd-decorated VO<sub>2</sub> nanowire biased at 5 V causes the current to increase steadily up to ~ 3 min of H<sub>2</sub> exposure and then increase abruptly to ~ mA. If the series resistor is not taken into account, the giant resistance change of the nanowire can be as high as 4 orders of magnitude. As the Pd thickness increases to 2 nm, such abrupt change in current occurs less than 1 min of H<sub>2</sub> exposure. Interestingly, they both display abrupt changes at the same current level of approximately 30  $\mu$ A. Previously, we argued that the spillover of catalytically produced H atoms onto a VO<sub>2</sub> nanowire contributed to its carrier concentration, triggering the MIT, considered as Mott-Hubbard type.

When 3 nm Pd was deposited and annealed (highly-dense Pd nanoparticles were seen to be well-dispersed, as shown in the inset of the Figure 3.17a), the current abruptly increases to ~ 1mA from 1.5  $\mu$ A after H<sub>2</sub> exposure without delay. The details of the current dependence with exposure time are shown in Figure 3.17 (b). The current increases very fast with exposure time after a little drop (1.5  $\mu$ A to 1.1  $\mu$ A) in current and reach its metallic phase after 4 s of H<sub>2</sub> exposure. It is worth noting that the current at which the insulator to metal transition occurs is very low and the transition is done slowly for several seconds, unlike a typical timescale of the transition (~ picoseconds or faster).

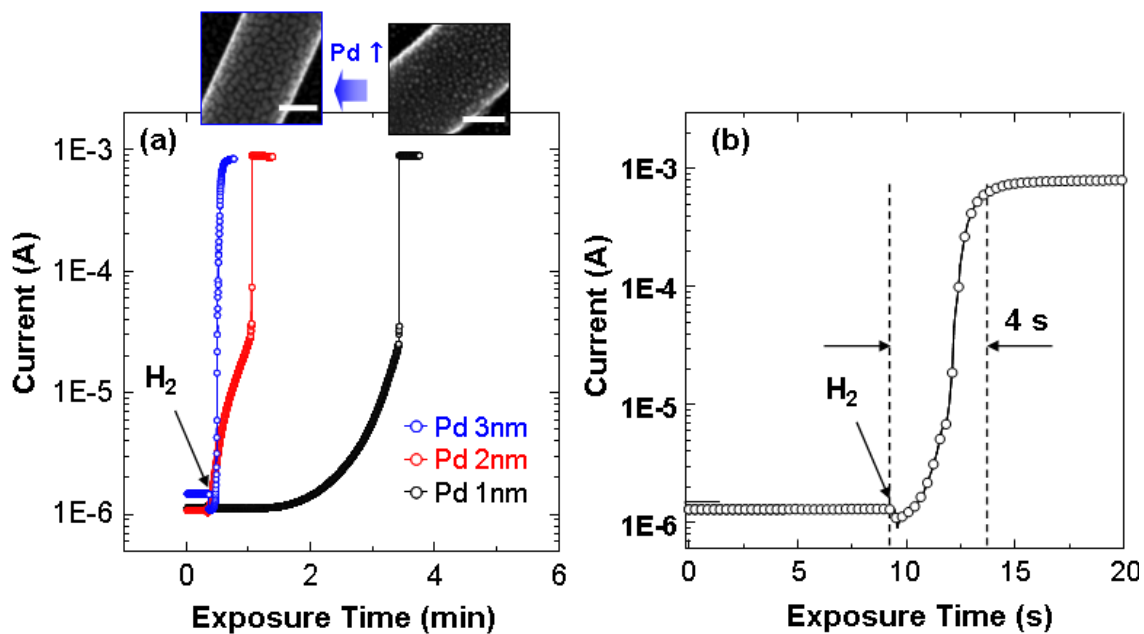


Figure 3.17(a) The change in current for a Pd-decorated VO<sub>2</sub> nanowire biased at 5 V as a function of time of exposure to hydrogen gas with Pd film thickness (1 – 3 nm). The scale bar in the inset is 100 nm. As the Pd thickness is increased from 1 to 3 nm, the hydrogen response becomes faster.(b) The details of the current change of Pd-VO<sub>2</sub> nanowire, exposed to hydrogen flowing at 5 sccm added for various lengths of time to a 1000 sccm background air stream with the thickness of Pd films.

### 3.2.15. Response rate with hydrogen concentration

Figure 3.18 shows  $I_D$  curves for a Pd-decorated  $\text{VO}_2$  nanowire at  $50^\circ\text{C}$  exposed to varying hydrogen concentration in dry air ranging from 250 ppm to 5000 ppm. When the Pd-decorated  $\text{VO}_2$  nanowire biased at 5V is exposed to hydrogen, the current abruptly increases from insulating phase to metallic phase without delay. With a  $\text{H}_2$  concentration of 5000 ppm, the response time was measured to be less than 5 s. As the hydrogen concentration decreases, the rate of increase in a current becomes slow and the response time decreases exponentially with the  $\text{H}_2$  concentration (Figure 3.18b). With a  $\text{H}_2$  concentration of 250 ppm, it is observed that the transition can occur within 30 sec.

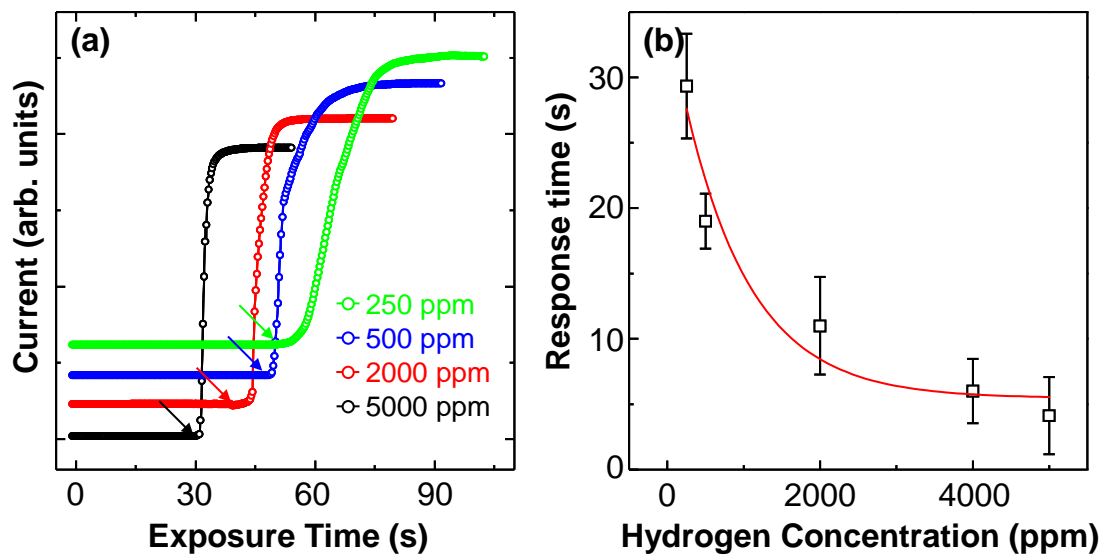


Figure 3.18(a)  $I_D$  curves for a Pd-decorated  $\text{VO}_2$  nanowire at  $50^\circ\text{C}$  exposed to varying hydrogen partial pressures in dry air corresponding to concentrations ranging from 250 ppm to 5000 ppm. (b) The rate of increase in a current with hydrogen concentration.

### 3.2.16. Response rate with palladium distance

In order to see the influence of the Pd coverage on the current response, we analyzed a quantitative relationship between the distance between Pd nanoparticles, and the response time was plotted with the H<sub>2</sub> concentration of 500 and 5000 ppm (Figure 3.19). As indicated in the Figure 3.17 (a), when the Pd nanoparticles are well-dispersed and the distance between Pd nanoparticles is very short (< 3 nm), the transition occurs within 1-2 s. Very similar results were obtained with over 10 devices fabricated and measured independently. As the distance increase, the response time increases quite linearly. At a distance less than 10 nm, the device show similar current response behavior. This result was also achieved at hydrogen concentration of 500 ppm although the rate of increase in the response time is slower.

Dissociative chemisorption of hydrogen on Pd surfaces followed by the subsequent incorporation as atomic hydrogen in the Pd crystal to form a solid hydride is a well-known process. At low hydrogen concentrations up to PdH<sub>0.02</sub>, the lattice expands slightly from 3.889 Å to 3.895 Å. Above this concentration the second phase appears with a lattice constant of 4.025 Å. This volume expansion at high Pd coverage may make percolating PdH<sub>x</sub> nanoparticles, forming an electrically continuous film.<sup>[58]</sup> The observed changes in current can be thus related to metal percolation occurring on the nanowire's surface. However, on termination of the hydrogen exposure, the recovery of the conductance toward its initial value was found to be very slow. Even after 1 h at 50 °C in air, the conductance did not change significantly. The irreversibility of the current response is not usually found in the Pd percolating sensors which show fast recovery within 1 min.

The hydrogen atoms also spill over the VO<sub>2</sub> nanowire's surface and then diffuse into the vanadium oxide, forming the hydrogen interstitials or adsorbed OH, both of which act as electron donors increasing the carrier density in the conduction band. At low Pd coverage, the carrier density increase with hydrogen exposure time is initially observed as a steady conductance increase of the nanowire while in its insulator phase in Figure 3.17 (a). If it is responsible for the abrupt increase in the conductance observed at high Pd coverage, an ultrafast (<nsec) transition after the steady conductance increase should be seen at approximately 30 μA, as shown at low Pd coverage. Furthermore, the diffusion of hydrogen atoms into Pd is much faster (~ 8 orders) than that into VO<sub>2</sub>,<sup>[38]</sup> suggesting that the diffusion into the Pd is essentially complete when those involving the oxide are just beginning. The diffusion of hydrogen atoms into the VO<sub>2</sub> would not produce so large a current increase in so short a time at such a low temperature (323K).

Now, we focus on the Pd-H reaction again. The process is well-known to be exothermic with a heat of reaction of about 9.5 Kcal/mole of H<sub>2</sub> at around 25 °C,<sup>[59]</sup> which heats locally the underlying region. For VO<sub>2</sub>-based two-terminal devices, the first-order metal-insulator transition, accompanied by

several orders of magnitude jump in conductivity, is usually observed when single-crystalline VO<sub>2</sub> is heated uniformly. However, by such localized and nanoscale heating, metallic domains at the localized region underneath Pd nanoparticles will start to nucleate, coexisting metallic and insulating phases in VO<sub>2</sub>.<sup>[1, 60]</sup> These domains continue to grow and expand along VO<sub>2</sub> nanowires with hydrogen exposure time, resulting in markedly different current behavior at high Pd coverage. The growth rate of the metallic domains will depend on the Pd coverage and hydrogen concentration, as shown in Figures 3.18 and 3.19.

An inhomogeneous strain may be also induced by the periodic metal-insulator domain due to the difference in volume between metallic and insulating phases. Actually, if the VO<sub>2</sub> nanowire is strained compressively, the insulator to metal transition can be triggered at lower temperature than 68 °C in the bulk. Previously, a substrate effect wherein the strain arising from the mismatch of thermal expansion between VO<sub>2</sub> and SiO<sub>2</sub> result in alternating domains of metal and insulator regions of the VO<sub>2</sub> along the length of the nanowire was described.<sup>[61]</sup> The rather complex current v.s. temperature behavior, multiple transitions, was reported in that study. Although the substrate effects are excluded because the current responses in Figure 3.18 are also clearly seen in strain-free VO<sub>2</sub> nanowires transferred onto foreign SiO<sub>2</sub> substrate, the strain effects should be considered, and the magnitude of stress and the time rate of increase in stress will also depend on the Pd coverage and hydrogen concentration.

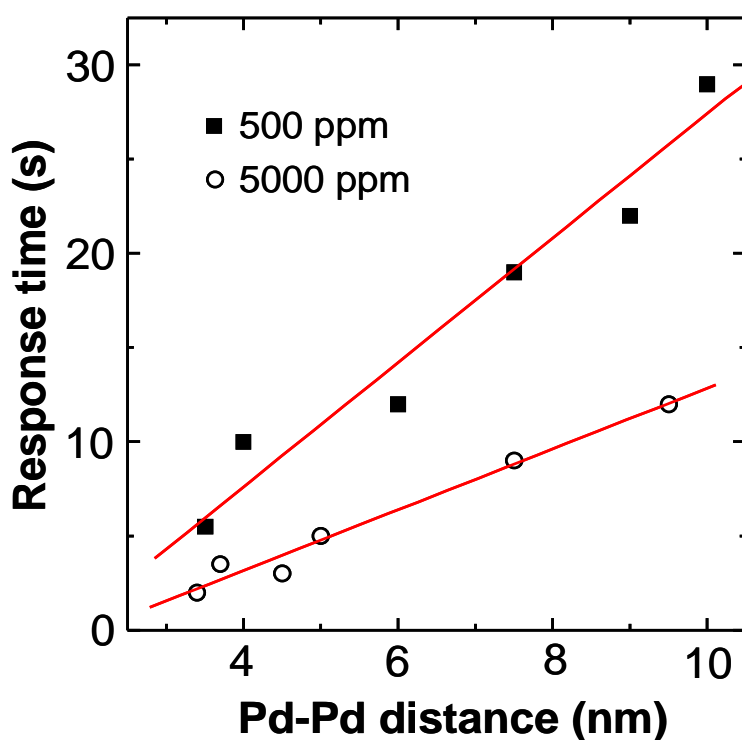


Figure 3.19 Response time with the H<sub>2</sub> concentration of 500 and 5000 ppm with Pd coverage.



### 3.2.17. Phase transition in VO<sub>2</sub> due to localized heating via Pd-H reaction

Which of the two processes, induced stress in VO<sub>2</sub> or localized thermal heating of Pd-H reactions by hydrogen adsorption into Pd nanoparticles is the rate-determining process may be obtained by performing finite element analyses using COMSOL Multiphysics software. For simplicity, we employ two dimensional models for VO<sub>2</sub> nanowires and Pd nanoparticles, and mimic the exothermal reaction of Pd and H atoms by assigning a heat source in each Pd nanoparticle. We solve a coupled equation of heat transfer and linear elasticity, but intentionally rule out the effect of Joule heating. In our simulations, the resistivity is computed as a function of temperature and induced thermal stress, using a reported form by Cao et al.<sup>[62]</sup>:

$$\rho(T, \sigma) = \rho_0 \exp\left(\frac{E_a + \gamma\sigma}{k_B T}\right)$$

and the threshold conductivity for the MIT is assigned to be 14 S/m. One can find the details in material properties and the parameters of the above equation in ref [63].

Using simple models, we investigate the basic characteristic of thermal diffusion in our systems, before analyzing a real dimension of VO<sub>2</sub> nanowires. By setting that the length and height of the nanowire are 4.8 and 0.2 μm respectively, Pd nanoparticles (0.4 μm in length and 0.02 μm in height) are decorated the surface of VO<sub>2</sub> nanowire. In Figure 3.20 (a), temperature (or compressive stress) shows a local distribution until ~50 nsec, but it reaches to the bottom surface and becomes uniform throughout the height within ~100 nsec. This time scale for thermal diffusion is very short, and can be explained by the thermal diffusivity of VO<sub>2</sub> (~ 8.4 × 10<sup>5</sup> μm<sup>2</sup>/s). We further compare the temperature distributions in the nanowire for differently decorated Pd nanoparticles. When Pd atoms are deposited as a thin film with uniform thickness, the temperature profile shows a quadratic function along the length. However, Pd atoms are decorated as a form of particles like in our system, the temperature profile changes to the combination of piecewise linear and quadratic curves. Here, in the region with a bare surface, the temperature changes linearly, but it shows a quadratic change in the region covered by a Pd particle, as shown in Figure 3.21 (a). It is notable that both temperature profiles have the maximum at the center of the nanowire. In addition, we compare the temperature profiles with different sizes of Pd nanoparticles. For this, the same amount of Pd nanoparticles with different sizes (10 nm and 200 nm) deposited on the top surface of the same VO<sub>2</sub> nanowires, and the total numbers of Pd particles are 100 and 5, respectively. As shown in Figure 3.21 (b), the global temperature profiles are almost the same, though there is small deviation locally. It indicates that the total amount of Pd nanoparticles is a dominant factor rather than the size of nanoparticles for the thermal heating. Based on these results, we model the Pd particles with micrometer size for later calculations for efficiency.

We calculated the changes of temperature, compressive stress, and conductivity of VO<sub>2</sub> nanowires by varying the length of VO<sub>2</sub> nanowire from 24 μm to 198 μm, as shown in Figure 3.20 (b). Here, the heat source per a single Pd atom is 1 eV/s, the size of Pd particle is 2 μm, and the inter-distance between Pd particles is 4 μm. For the 198 μm long nanowire, the initiation of the MIT transformation at t = 13.5 sec is observed in the center of the wire, but we don't see any transformation for shorter nanowires up to t = 20 sec. In contrast, the maximum compressive stress induced by localized thermal heating is found to be at most ~100MPa even for the longest nanowire, which can make only a small change of conductivity, and thus lower the critical temperature of the MIT less than 1°C. This indicates that the change in the current for Pd-decorated VO<sub>2</sub> nanowires exposed to hydrogen gas in Figures 3.17 and 3.18 is attributed to the increase of temperature due to the localized heating, rather than the compressive stress. However, we have to mention that we need to employ sufficiently long nanowires to detect the H<sub>2</sub> molecules using the MIT induced by the exothermal reaction. This may imply that the experimental values have to consider the limitations of the electronic response of the measurement system and the rate of hydrogen injection into a chamber.

Assuming that Pd-H reaction is constant with time, the heat sources of 0.25, 0.50, 0.75 and 1.00 eV/s per a single Pd atom are applied until they reach to the net heat of 30 eV per a single Pd atom. These values are relatively higher than the heat of reaction of palladium hydrides, but it can be compensated by an additional heat by Joule heating which we do not consider in our calculations. The profiles of temperature and the corresponding electrical conductivity at t = 20 sec are shown in Figure 2.21 in the Supporting Information. The increment of temperature is proportional to the amount of heat source. The MIT is initiated at a critical heat source of 0.68eV/s at t = 20 sec, and thus the critical amount of heat is 13.6 eV per a single Pd atom to induce the MIT at the 198 μm nanowire. We also change the size of Pd particles from 1 μm to 4 μm and the distance from 2μm to 5μm. The total numbers of Pd particles are the same, and thus the covered areas are different. In the profiles of temperature and electric conductivity at t = 20 sec (Figure 3.21), as the coverage increases the maximum temperature increases, consistent with the results in Figure 3.19. All calculations confirm that the generated heat by the exothermal reaction of Pd and H atoms can induce the MIT without the aid of Joule heating.

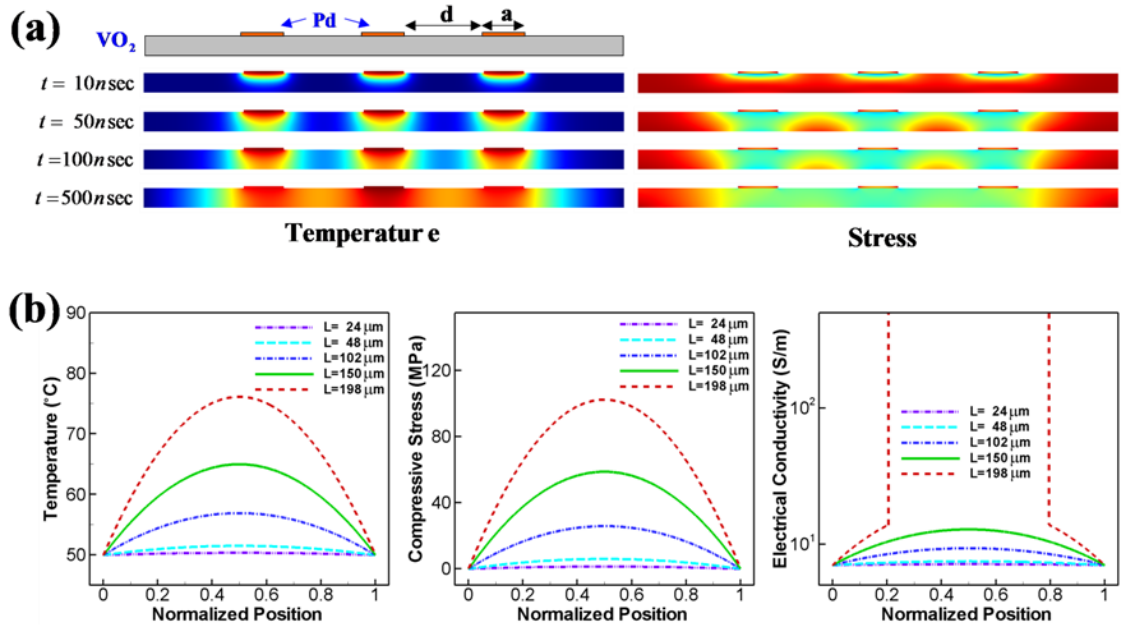


Figure 3.20(a) The snapshots of temperature and induced compressive stress distributions of  $\text{VO}_2$  nanowire by Pd-H exothermal reaction. (b) The profiles of temperature, induced compressive stress, and conductivity of  $\text{VO}_2$  nanowires with different length.

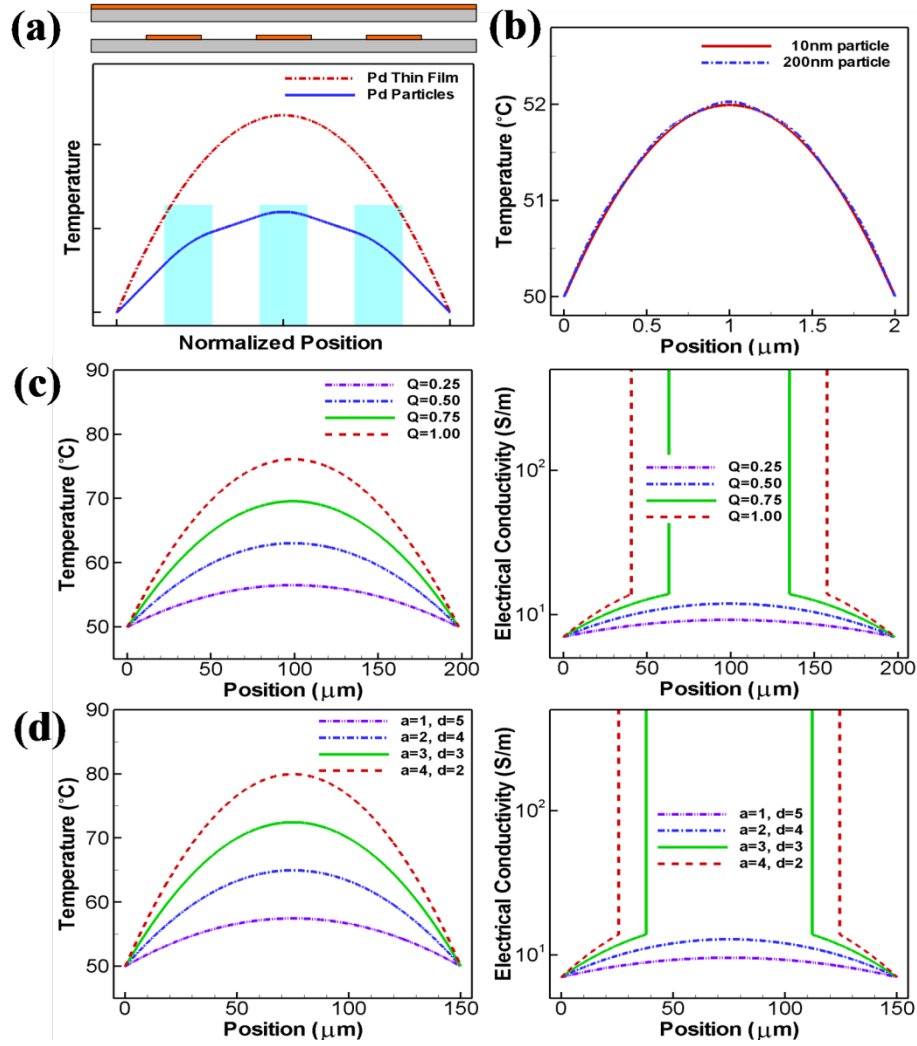


Figure 3.21 Comparison of temperature profiles of VO<sub>2</sub> nanowires decorated by a Pd thin film and Pd nanoparticles in (a) and that decorated by 10nm size Pd nanoparticles and 200nm size Pd nanoparticles in (b) The profiles of temperature and conductivity for different amount of heat sources per a single Pd atom in (c) and those for different sizes and inter-distances of Pd nanoparticles in (d).

### 3.2.18. Two recovery methods following hydrogen flow

After hydrogen flow is shut off, the recovery of the nanowire's conductance toward its initial value was found to be very slow.<sup>[38]</sup> To reduce the recovery time, we employed two types of recovery process, which to heat the sample at 100 ~ 200 °C (Figure 3.22a) and to stretch the sample (Figure 3.22b). The heating process still requires over several minutes at 100 °C (Figure 3.23).<sup>[38]</sup> However, when the substrate was stretched, the current abruptly dropped to the initial value within less than 0.1 sec, depending on the rate and magnitude of stress, suggesting the possibility as flexible gas sensor applications.

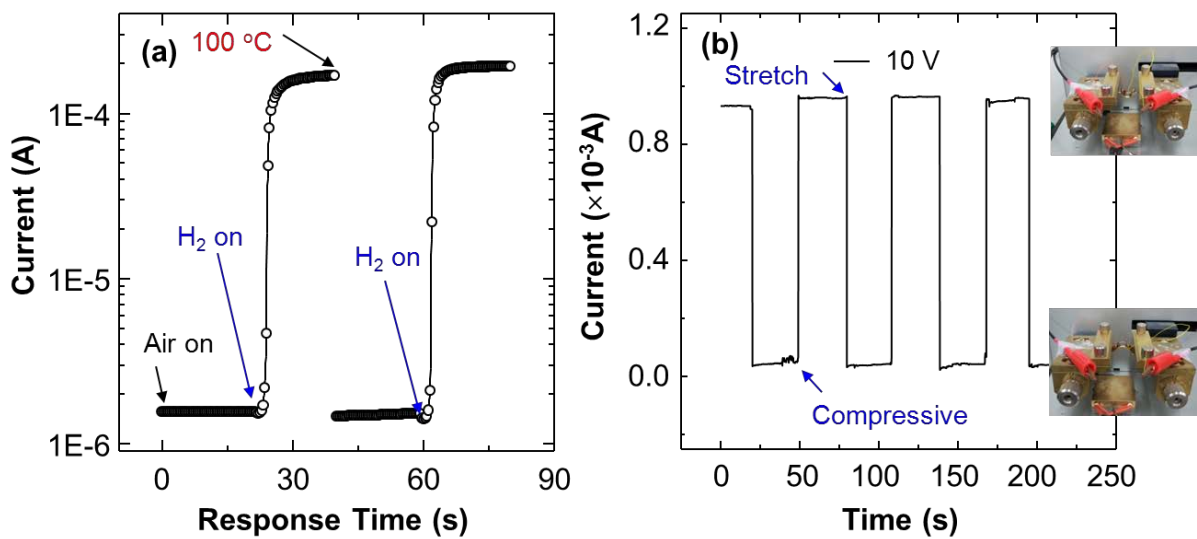


Figure 3.22 Two types of recovery process, heat the sample at 100 ~ 200 °C (a) and stretching the sample (b).

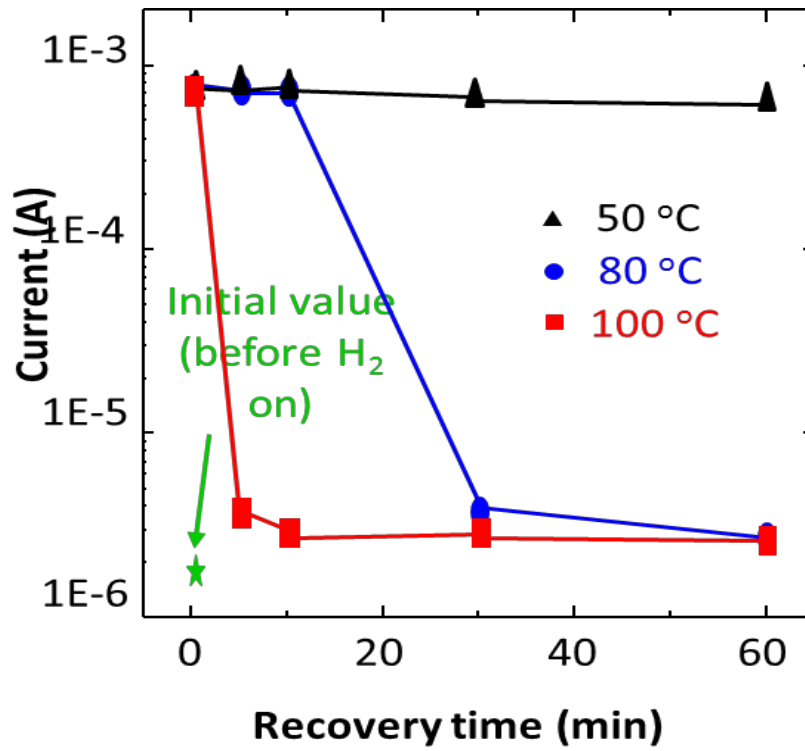


Figure 3.23 The change in current for a Pd-decorated VO<sub>2</sub> nanowire after hydrogen off with annealing temperature.

### 3.2.19. Sensing performance at the low voltage and room temperature

More interestingly, one observe that this device could even operate at room temperature if we apply 10 V to the nanowires although the response time increased up to 3 ~ 4 min (Figure 3.24a). The voltage may provide a high power that can come close to the  $T_c$  to trigger the transition. The self-heating effect to drive the transition was reported in the study in the strain monitor.<sup>[60]</sup> However, the current already increases to 2 times within 10 s of hydrogen exposure, meaningful as a hydrogen sensor. It is also interesting that after hydrogen exposure, the current abrupt decreased to 0.5  $\mu\text{A}$  (1 order in magnitude decrease), which are currently being investigated, will be the subject of a separate publication. The operating voltage can be reduced to 0.1 V at ambient temperature of 50  $^\circ\text{C}$  (Figure 3.24b). Because the power consumption is proportional to the square of the device's supply voltage, which should therefore be kept as low as possible, the devices at 0.1 V consumes 250 times less power than those at 5 V.

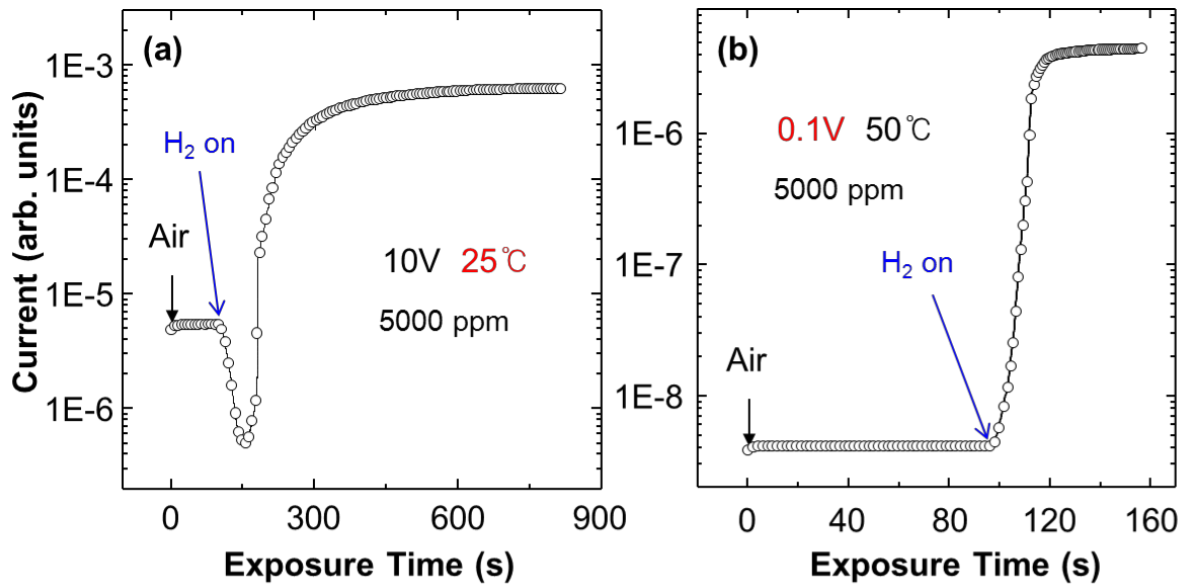


Figure 3.24 The change in current for a Pd-decorated VO<sub>2</sub> nanowire biased at 10 V with exposure to hydrogen gas at room temperature (a) a Pd-decorated VO<sub>2</sub> nanowire biased at 0.1 V at 50  $^\circ\text{C}$  (b).

### 3.3. CONCLUSIONS

In summary, we demonstrated that increasing the conductivity was one of effective methods for accelerating the response and reducing the operating temperature of an MIT based hydrogen sensor. By irradiating a well-controlled electron beam into the nanowires, the conductivity of nanowires significantly increases up to 4 times with little change in the insulator to metal transition temperature ( $< 2\text{ }^{\circ}\text{C}$ ). The conductivity is further increased when exposed to trace amounts of hydrogen gas, inducing the insulator to metal transition after several minutes. As the conductivity increases, the transition to metallic phase can occur faster ( $\sim 2\text{ x}$ ) even near room temperature ( $\sim 35\text{ }^{\circ}\text{C}$ ), by reaching faster ( $\sim 3\text{ x}$ ) a critical current density at which the self-heating initiates. The self-heating effect accelerated by the increase in the conductivity results in a decrease of response time, in the operating temperature and voltage. The sensor also shows the capability of selectively detecting hydrogen gas from ( $\text{O}_2$ ,  $\text{CO}$ , and ethylene) gases. If catalytic nanoparticles interacting strongly with specific gases are designed with optimization and properly decorated onto  $\text{VO}_2$  nanowires, such highly responsive ( $\sim 1000$ -fold sensitivity) and highly selective sensors can be easily fabricated without arrays of sensors.

Also, we reported an unusual insulator to metal transition of the palladium-decorated  $\text{VO}_2$  nanowires caused by the heterogeneous  $\text{H}_2$ -Pd catalytic reactions. The Pd- $\text{VO}_2$  showed an abrupt increase in conductance from insulator to metal at lower temperature ( $\sim 50\text{ }^{\circ}\text{C}$ ) than  $68\text{ }^{\circ}\text{C}$  in the bulk on hydrogen gas exposure. The abrupt change occurred smoothly over duration of several seconds to several tens of seconds, depending on the Pd coverage, temperature, and hydrogen concentration. Electronic transport measurements and finite element analyses with various experimental conditions such as hydrogen concentration, temperature, Pd coverage, and applied voltage suggest that the deceleration in the transition is due to the formation of alternating domains of metal and insulator regions of the  $\text{VO}_2$ , which were produced by the generated heat by the exothermic catalytic process. *Although* the nanoscale heating may be negligible in gas sensor materials such as  $\text{ZnO}$  and  $\text{SnO}_2$  etc, it is believed to be quite enough for triggering the transition along the nanowires at ambient temperature close to the insulator to metal transition temperature in the bulk.

After hydrogen flow is shut off, the conductance is not immediately returned to the original value and it takes 30 min even after  $100\text{ }^{\circ}\text{C}$ , meaning that the atomic hydrogens, produced by dissociative chemisorption on Pd, are incorporated into  $\text{VO}_2$ . However, the Pd-decorated  $\text{VO}_2$  nanowire after the recovery process also shows similar current response to hydrogen, meaning that it is reversible. This has critical implications for the engineering the properties of vanadium dioxide by a heterogeneous catalytic process.



## References

- [1] Cao, J.; Ertekin, E.; Srinivasan, V.; Fan, W.; Huang, S.; Zheng, H.; Yim, J.W. L.; Khanal, D. R.; Ogletree, D. F.; Grossman, J. C.; Wu, J. *Nat. Nanotech.* **2009**, *4*, 732-737.
- [2] Lazarovits, B.; Kim, K.; Haule, K.; Kotliar, G. *Phys. Rev. B.* **2010**, *81*, 115117.
- [3] Cao, J.; Gu, Y.; Fan, W.; Chen, L. Q.; Ogletree, D. F.; Chen, K.; Tamura, N.; Kunz, M.; Barrett, C.; Seidel, J.; Wu, J. *Nano Lett.* **2010**, *10*, 2667-2673.
- [4] Tselev, A.; Budai, J. D.; Strelcov, E.; Tischler, J. Z.; Kolmakov, A.; Kalinin, S. V. *Nano Lett.* **2011**, *11*, 3065-3073.
- [5] Wu, Junqiao.;Gu, Qian.; Guition, S, Beth.; Leon, Nathalie, P de. ; Ouyang, Lian. Park, Hongkun. *Lett.* **2006**, *6*, 2313-2317.
- [6] Eyert, V. *Ann. Phys. (Berlin)***2002**, *11* (9), 650-704.
- [7] Marezio, M., ; McWhan, B. ; Dernier, P, D. ; Remeika, J. P. *Phys. Rev. B***1972**, *5* (7), 2541-2551
- [8] Pouget, J. P.; Launois, H.; D'Haenens, J. P.; Merenda, P.; Rice, T. M. *Phys. Rev. Lett.* **1975**, *35*, 873-875.
- [9] Sohn, J. I.; Joo, H. J.; Ahn, D.; Lee, H. H.; Porter, A. E.; Kim, K.; Kang, D. J.; Welland, M. E. *Nano Lett.* **2009**, *9*, 3392-3397.
- [10] Zhang, S.; Chou, J. Y.; Lauhon, L. J. *Nano Lett.* **2009**, *9*, 4527-4532.
- [11] Booth, J. M.; Casey, P. S. *ACS Appl. Mater. Interfaces* **2009**, *1*, 1899-1905.
- [12] Jones, A.; Berweger, S.; Wei, J.; Cobden, D. H.; Raschke, M. *Nano Lett.* **2010**, *10*, 1574-1581.
- [13] Cao, J.; Ertekin, E.; Srinivasan, V.; Fan, W.; Huang, S.; Zheng, H.; Yim, J.W. L.; Khanal, D. R.; Ogletree, D. F.; Grossman, J. C.; Wu, J. *Nat. Nanotech.* **2009**, *4*, 732-737.
- [14] Cao, J.; Gu, Y.; Fan, W.; Chen, L. Q.; Ogletree, D. F.; Chen, K.; Tamura, N.; Kunz, M.; Barrett, C.; Seidel, J.; Wu, J. *Nano Lett.* **2010**, *10*, 2667-2673.
- [15] Zhang, Shixiong.; Chou, Jung, Yen.; Lauhon, Lincoln, J. *Nano Lett.* **2009**, *9*, 4527-4532

- [16] Kim, Hyeongkeun.; Kim, Yena.; Kim, Keun, Soo.; Jeong, Hu Young.; Jang, A-Rang.; Han, Seung, Ho.; Yoon, Dae, Ho.; Suh, Kwang, S.; Shin, Hyeon, Suk.; Kim Tae, Young.; Yang, Woo, Seok. *ACS Nano*. **2013**, *7*, 5769-5776.
- [17] Parkin, I. P.; Manning, T. D. *J. Chem. Educ.* **2006**, *83*, 393–400.
- [18] Zhang, Z.; Gao, Y.; Luo, H.; Kang, L.; Chen, Z.; Du, J.; Kanehira, M.; Zhang, Y.; Wang, Z. L. *Energy Environ. Sci.* **2011**, *4*, 4290–4297.
- [19] Xu, G.; Huang, C.-M.; Tazawa, M.; Jin, P.; Chen, D.-M.; Miao, L. *Appl. Phys. Lett.* **2008**, *93*, 061911.
- [20] Mott, N. F. *Proc. Phys. Soc. (London)* **1949**, *A62*, 416.
- [21] Mott, N. F. *ReV. Mod. Phys.* **1968**, *40* (4), 677–683.
- [22] Kim, H, T. *NATO Science Series*. **2002**,*II/67*, 137-153;online at <http://xxx.lanl.gov/abs/cond-mat/0110112>.
- [23] W. F. Brinkman and T. M. Rice, *Phys. Rev.* **1970**, *B2*, 4302.
- [24] Kim, H, T.; Chae, B, G.; Youn D, H.; Maeng, S, L.; Kim, G.; Kang K, Y.; Lim Y, S. *New. J. Phys.* **2004**, *6*, 52
- [25] Huang, M. H.; Mao, S.; Feik, H.; Yan, H. Q.; Wu, Y. Y.; Kind, H.; Weber, E.; Russo, R.; Yang,P. D. *Science***2001**, *292*, 1897-1899.
- [26] Law, M.; Greene, L. E.; Johnson, J. C.; Saykally, R.; Yang, P. D. *Nat. Mater.* **2005**, *4*, 455-459.
- [27] Stem, E.; Klemic, J. F.; Routenberg, D. A.; Wyrembak, P. N.; Turner-Evans, D. B.; Hamilton,A. D.; LaVan, D. A.; Fahmy, T. M.; Reed, M, A. *Nature***2007**, *445*, 519-522.
- [28] Ham, J. H.; Shim, W. Y.; Kim D. H.; Lee, S. H.; Roh, J. W.; Sohn, S. W.; Oh, K, H.; Voorhees,P. W.; Lee, W. Y. *Nano Lett.* **2009**, *9*, 2867-2872.
- [29] Kolmakov, A.; Moskovits, M. *Ann. Rew. Mater. Res.* **2004**, *34*, 151-162.
- [30] Gratzel, M. *Nature***2001**, *414*, 338-344.
- [31] Strelcov, E.; Lilach, Y.; Kolmakov, A. *Nano Latt.* **2009**, *9*, 2322-2326.

- [32] Goodenough, J. B. *Phys. Rev.* **1960**, *117*, 1442-1451.
- [33] Zylbersztein, A.; Mott, N. F. *Phys. Rev. B* **1975**, *11*, 4383-4395.
- [34] Cavalleri, A.; Dekorsy, Th.; Chong, H.H.W.; Kieffer, J.C.; Schoenlein, R.W. *Phys. Rev. B* **2004**, *70*, 161102.
- [35] Kim, H.-T.; Kim, B.-J.; Lee, Y. W.; Chae, B.-G.; Yun, S. J.; Kang, K.-Y. Hole driven MIT theory, *Physica C: Superconductivity and its Applications* **2007**, 460-462, 1076-1078.
- [36] Wei, J.; Ji, H.; Guo, W.; Nevidomskyy, A. H.; Natelson, D. *Nat. Nanotech.* **2012**, *7*, 357-362.
- [37] Wu, C.; Feng, F.; Feng, J.; Dai, J.; Peng, L.; Zhao, J.; Yang, J.; Si, C.; Wu, Z.; Xie, Y. *J. Am. Chem. Soc.* **2011**, *133*, 13798-13801.
- [38] Baik, J. M.; Kim, M. H.; Larson, C.; Yavuz, C. T.; Stucky, G. D.; Wodtke, A. M.; Moskovits, M. *Nano Lett.* **2009**, *9*, 3980-3984.
- [39] Varghese, B.; Tamang, R.; Tok, E. S.; Mhaisalkar, S. G.; Sow, C. H. *J. Phys. Chem. C* **2010**, *114*, 15149-15156.
- [40] Yang, Z.; Ko, C.; Ramanathan, S. *Annu. Rev. Mater. Res.* **2011**, *41*, 337-367.
- [41] Gaidi, M.; Chenevier, B.; Labeau, M. *Sens. Actuators, B* **2000**, *62*, 43-48.
- [42] Ryzhikov, A. S.; Shatokhin, A. N.; Putilin, F. N.; Rumyantseva, M. N.; Gaskov, A. M.; Labeau, M. *Sens. Actuators, B* **2005**, *107*, 387-391.
- [43] Baik, J. M.; Zielke, M.; Kim, M. H.; Turner, K. L.; Wodtke, A. M.; Moskovits, M. *ACS Nano* **2010**, *4*, 3117-3122.
- [44] Syed, M.; Moskovits, M. *Adv. Mater.* **2011**, *23*, 2306-2312.
- [45] Chaez, B. G.; Kim, H. T.; Yun, S. J. *Electrochem. Solid-State Lett.* **2008**, *11*, D53- D55.
- [46] Lee, S.; Cheng, C.; Guo, H.; Hippalgaonkar, K.; Wang, K.; Suh, J.; Liu, K.; Wu, J. *J. Am. Chem. Soc.* **2013**, *135*, 4850-4855.
- [47] Zhang, S.; Kim, I. S.; Lauhon, L. J. *Nano Lett.* **2011**, *11*, 1443-1447.

- [48] Ilinskiya, A. V.; Kvashenkinab, O. E.; Shadrina, E. B. *Semiconductors*, **2012**, *46*, 422-429.
- [49] Ji, H.; Wei, J.; Natelson, D. *Nano Lett.* **2012**, *12*, 2988–2992.
- [50] Hong, W.; Park, J. B.; Yoon, J.; Kim, B.; Sohn, J. I.; Lee, Y. B.; Bae, T.; Chang, S.; Huh, Y. S.; Son, B.; Stach, E. A.; Lee, T.; Welland, M. E. *Nano Lett.* **2013**, *13*, 1822–1828.
- [51] Baik, J. M.; Kim, M. H.; Larson, C.; Wodtke, A. M.; Moskovits, M. *J. Phys. Chem. C* **2008**, *112*, 13328–13331.
- [52] Whittaker, L.; Wu, T. L.; Patridge, C. J.; Sambandamurthy, G.; Banerjee, S. *J Mater. Chem.* **2011**, *21*, 5580-5592.
- [53] Nagashima, M.; Wada, H.; Tanikawa, K. Shirahata, H. *Jpn. J. Appl. Phys.* **1998**, *37*, 4433-4438.
- [54] Strelcov, E.; Dmitriev, S.; Button, B.; Cothren, J.; Sysoev, V.; Kolmakov, A. *Nanotechnology*, **2008**, *19*, 355452.
- [55] Hu, B.; Zhang, Y.; Chen, W.; Xu, C.; Wang, Z. L. *Adv. Mater.* **2011**, *23*, 3536-3541.
- [56] Nishikawa, M.; Nakajima, T.; Manabe, T.; Okutani, T.; Tsuchiya, T. *Mater. Lett.* **2010**, *64*, 1921-1924.
- [57] Crunteanu, A.; Givernaud, J.; Leroy, J.; Mardivirin, D.; Champeaux, C.; Orlianges, J. – C.; Catherinot, A.; Blondy, P. *Sci. Technol. Adv. Mater.* **2010**, *11*, 065002.
- [58] Kolmakov, A.; Chen, X.; Moskovits, M. *J. Nanosci. Nanotechnol.* **2008**, *8*, 111-121.
- [59] Lewis, F. A. *Platinum Metals Rev.* **1960**, *4*, 132-137.
- [60] Hu, B.; Chen, Z. W.; Xu, C.; Wang, Z. L. *Adv. Mater.* **2011**, *23*, 3536-3536.
- [61] Wu, J.; Gu, Q.; Guiton, B. S.; de Leon, N. P.; Ouyang, L.; Park, H. *Nano Lett.* **2006**, *6*, 2313-2317.
- [62] Cao, J.; Fan, W.; Chen, K.; Tamura, N.; Kunz, M.; Eyert, V.; Wu, J. *Phys. Rev. B* **2010**, *82*, 241101(R).
- [63] Byon, J. W.; Kim, M.-B. Kim, M. H.; Kim, S. Y.; Lee, S. H.; Lee, B. C.; Baik, J. M. *J. Phys. Chem. C*, **2012**, *116*, 226–230.

## **Acknowledgement**

I would never have been able to finish my dissertation without the guidance of my committee members, help from friends, and support from my family.

I would like to express my deepest gratitude to my advisor, Prof. Dr. Baik, for his excellent guidance, caring, patience, and providing me with an excellent atmosphere for doing research. The deepest gratitude is also due to the members of the supervisory committee, Prof. Dr. Choi and Prof. Dr. Song. Without their knowledge and assistance, this study would not have been successful.

Specially, I wish to thank all my graduate friends, especially members; Dr. Joon Mo Park, Jin Sung Chun, Byeong Uk Ye, Won Jeong Park, Ji Hyeon Kim, Kyeong Nam Kim, Jae Won Lee, Min Jin Kim, Hee Jun Kim, and Byeong Uk Park for sharing the literature and invaluable assistance.

Finally, I am appreciated to my family – parents and two older sisters. They were always supporting me and encouraging me with their best wishes.